Intelligent Reflecting Surface Enabled Sensing: Cramér-Rao Bound Optimization

Xianxin Song , *Graduate Student Member, IEEE*, Jie Xu , *Senior Member, IEEE*, Fan Liu , *Member, IEEE*, Tony Xiao Han, *Senior Member, IEEE*, and Yonina C. Eldar , *Fellow, IEEE*

Abstract—This article investigates intelligent reflecting surface (IRS) enabled non-line-of-sight (NLoS) wireless sensing, in which an IRS is deployed to assist an access point (AP) to sense a target at its NLoS region. It is assumed that the AP is equipped with multiple antennas and the IRS is equipped with a uniform linear array. We consider two types of target models, namely the point and extended targets, for which the AP aims to estimate the targets direction-of-arrival (DoA) and the target response matrix with respect to the IRS, respectively, based on the echo signals from the AP-IRS-target-IRS-AP link. Under this setup, we jointly design the transmit beamforming at the AP and the reflective beamforming at the IRS to minimize the Cramér-Rao bound (CRB) on the estimation error. Towards this end, we first obtain the CRB expressions in closed form. It is shown that for the point target, the CRB for estimating the DoA depends on both the transmit and reflective beamformers; while for the extended target, the CRB for estimating the target response matrix only depends on the transmit beamformers. Next, we optimize the joint beamforming design to minimize the CRB for the point target via alternating optimization, semi-definite relaxation, and successive convex approximation. We also obtain the optimal transmit beamforming solution in closed form to minimize the CRB for the extended target. Numerical results show that for both cases, the proposed designs based on CRB minimization achieve improved sensing performances than other traditional schemes.

I. INTRODUCTION

INTEGRATING wireless (radar) sensing into future beyond-fifth-generation (B5G) and six-generation (6G) wireless networks as a new functionality has attracted growing research interest to support various environment-aware applications such as industrial automation, auto-driving, and remote healthcare (see, e.g., [2], [3], [4] and the references therein). Conventionally, wireless sensing relies on line-of-sight (LoS) links between the access points (APs) and the sensing targets, such that the sensing information (e.g., the distance/velocity/angle of targets) can be extracted based on the target echo signals [3]. However, in practical scenarios with dense obstructions such as autonomous driving and smart city, sensing targets are likely to be located at the non-LoS (NLoS) region of APs, where conventional LoS sensing may not be applicable in general. Therefore, how to realize NLoS sensing in such scenarios is a challenging task.

Motivated by its success in wireless communications [5], [6], [7], [8], intelligent reflecting surface (IRS) or reconfigurable intelligent surface (RIS) has become a viable new solution to overcome this issue (see, e.g., [9], [10], [11], [12], [13], [14], [15], [16]). By properly deploying IRSs around the AP to recon\ the radio propagation environment, virtual LoS links are established between the AP and the targets in its NLoS region, such that the AP can perform NLoS target sensing based on the echo signals from AP-IRS-target-IRS-AP links. To combat the severe signal propagation loss over such triple-reflected links, the IRS can adaptively control the phase shifts at reflecting elements, such that the reflected signals are beamed towards desired target directions to enhance sensing performance.

There have been several prior works investigating IRS-enabled wireless sensing [9], [10], [11], [12], [13] and IRS-enabled integrated sensing and communications (ISAC) [14], [15], [16], respectively. For instance, the work [9] presented the NLoS radar equation based on the AP-IRS-target-IRS-AP link and evaluated the resultant sensing performance in terms of signal-to-noise ratio (SNR) and signal-to-clutter ratio (SCR). In [10], the authors considered an IRS-enabled bi-static target estimation, where dedicated sensors were installed at the IRS for estimating the direction of its nearby target through the IRS controller-IRS-target-sensors and IRS controller-target-sensors links. Under this setup, the authors optimized the IRS's reflective beamforming to maximize the average received signal power at the sensors. In [11], [12], [13], the authors considered IRS-enabled target detection, in which the IRS's passive beamforming was optimized to maximize the target detection

Xianxin Song and Jie Xu are with the School of Science and Engineering (SSE) and Future Network of Intelligence Institute (FNii), The Chinese University of Hong Kong (Shenzhen), Shenzhen 518172, China (e-mail: xianxinsong@link.cuhk.edu.cn; xujie@cuhk.edu.cn).

Fan Liu is with the Department of Electronic and Electrical Engineering, Southern University of Science and Technology, Shenzhen 518055, China (e-mail: liuf6@sustech.edu.cn).

Tony Xiao Han is with the Wireless Technology Lab, 2012 Laboratories, Huawei, Shenzhen 518129, China (e-mail: tony.hanxiao@huawei.com).

Yonina C. Eldar is with the Faculty of Mathematics and Computer Science, Weizmann Institute of Science, Rehovot 7610001, Israel (e-mail: yonina.eldar@weizmann.ac.il).

probability subject to a fixed false alarm probability constraint. In [14], the authors considered an IRS-enabled ISAC system with one base station (BS), one communication user (CU), and multiple targets, in which the IRS's minimum beampattern gain towards the desired sensing angles was maximized by jointly optimizing the transmit beamforming at the BS and the reflective beamforming at the IRS, subject to a minimum SNR requirement at the CU. In [15], [16], the authors considered an IRS-enabled ISAC system, in which the SNR of radar was maximized by joint beamforming design while ensuring a quality-of-service requirement at the CU.

In prior works on IRS-enabled sensing and IRS-enabled ISAC, the sensing SNR (or beampattern gain) and target detection probability have been widely adopted as the sensing performance measure for joint beamforming optimization. Cramér-Rao bound (CRB) is another important sensing performance measure, especially for target estimation tasks, which provides a lower bound on the variance of unbiased parameter estimators. In prior studies on wireless sensing [17], [18], [19] and ISAC [20], [21] without IRS, CRB has been widely adopted as the design objective for sensing performance optimization. Nevertheless, to our best knowledge, how to analyze the CRB performance for NLoS target estimation through the AP-IRS-target-IRS-AP link and optimize such performance by joint transmit and reflective beamforming design is still an uncharted area.

This article considers an IRS-enabled NLoS wireless sensing system, which consists of one AP with multiple antennas, one IRS with a uniform linear array (ULA), and one target at the NLoS region of the AP. It is assumed that the AP perfectly knows the channel state information (CSI) of the AP-IRS link, and the AP needs to estimate the target parameters based on the echo signals from the AP-IRS-target-IRS-AP link. We consider two types of target models [20], [22], [23], [24], namely the point and extended targets, respectively. For the point target scenario, the AP estimates the target's direction-of-arrival (DoA) with respect to (w.r.t.) the IRS. For the extended target scenario, the AP estimates the complete target response matrix w.r.t. the IRS (or equivalently the cascaded IRS-target-IRS channel matrix). We aim to minimize the CRB for parameters estimation, by jointly optimizing the transmit beamforming at the AP and the reflective beamforming at the IRS. The main contributions of the article are as follows:

- First, we obtain the closed-form CRB expressions for estimating the DoA and the target response matrix in the point and extended target cases, respectively. For the point target case, it is shown that the CRB depends on both the transmit and reflective beamformers, and the target's DoA can only be estimated when the rank of the AP-IRS or IRS-AP channel is larger than one or equivalently there are at least two signal paths. By contrast, for the extended target case, the target response matrix can only be estimated when the rank of the AP-IRS and IRS-AP channels are equal to the number of reflecting elements at the IRS, and the resultant CRB depends only on the transmit beamformers at the AP.

- Next, we minimize the obtained CRB by jointly optimizing the transmit beamforming at the AP and the reflective beamforming at the IRS, subject to a maximum power constraint at the AP. For the point target case, the formulated CRB minimization problem is non-convex and difficult to solve. We present an efficient algorithm via alternating optimization, semi-definite relaxation (SDR), and

successive convex approximation (SCA). For the extended target case, the resultant CRB minimization problem is convex, in which only the transmit beamforming vectors at the AP are optimization variables. We obtain the closed-form optimal transmit beamforming solution, in which the singular value decomposition (SVD) is first implemented to diagonalize the AP-IRS channel into parallel subchannels, and then channel amplitude inversion power allocation is performed over these subchannels.

- Finally, we present numerical results to validate the performance of our proposed designs. It is shown that the for the point target case, joint beamforming design based on CRB minimization achieves improved sensing performance in terms of mean squared error (MSE), as compared to traditional schemes with SNR maximization, transmit beamforming only, and reflective beamforming only. For the extended target case, the proposed transmit beamforming design outperforms the traditional isotropic transmission scheme. We also compare the CRB performance versus the MSE achieved by maximum likelihood estimation (MLE). For point target, the MSE converges towards the CRB when the SNR is sufficiently high. For extended target, the MSE equals the CRB.

The remainder of the article is organized as follows. Section II introduces the system model of our considered IRS-enabled NLoS wireless sensing system. Section III presents the closed-form CRB expressions for estimating the DoA and the target response matrix in the point and extended target cases, respectively. Section IV minimizes the CRB for estimating the DoA in the point target case by jointly optimizing the transmit beamforming at the AP and the reflective beamforming at the IRS. Section V minimizes the CRB for estimating the target response matrix in the extended target case by optimizing the transmit beamforming at the AP. Finally, Section VI provides numerical results, followed by a conclusion in Section VII.

Notations: Boldface letters refer to vectors (lower case) or matrices (upper case). For a square matrix $\mathbf{S}$, $\mathrm{tr}(\mathbf{S})$ and $\mathbf{S}^{-1}$ denote its trace and inverse, respectively, and $\mathbf{S} \succeq \mathbf{0}$ means that $\mathbf{S}$ is positive semi-definite. For an arbitrary-size matrix $\mathbf{M}$, $\mathrm{rank}(\mathbf{M})$, $\mathbf{M}^*$, $\mathbf{M}^T$, and $\mathbf{M}^H$ are its rank, conjugate, transpose, and conjugate transpose, respectively. The matrix $\mathbf{I}_m$ is an identity matrix of dimension m. We use $\mathcal{CN}(\mathbf{x}, \mathbf{\Sigma})$ to denote the distribution of a circularly symmetric complex Gaussian (CSCG) random vector with mean vector $\mathbf{x}$ and covariance matrix $\mathbf{\Sigma}$, and $\sim$ to denote "distributed as". The spaces of $x \times y$ complex and real matrices are denoted by $\mathbb{C}^{x \times y}$ and $\mathbb{R}^{x \times y}$, respectively. The real and imaginary parts of a complex number are denoted by $\mathrm{Re}\{\cdot\}$ and $\mathrm{Im}\{\cdot\}$, respectively. The symbol $\mathbb{E}(\cdot)$ is the statistical expectation, $\|\cdot\|$ stands for the Euclidean norm, $|\cdot|$ for the magnitude of a complex number, $\mathrm{diag}(a_1, \ldots, a_N)$ for a diagonal matrix with diagonal elements $a_1, \ldots, a_N$, $\otimes$ for the Kronecker product, $\mathrm{vec}(\cdot)$ for the vectorization operator, and $\mathrm{arg}(\mathbf{x})$ for a vector with each element being the phase of the corresponding element in $\mathbf{x}$.

II. SYSTEM MODEL

We consider an IRS-enabled NLoS wireless sensing system as shown in Fig. 1, which consists of one AP with $M_t > 1$ transmit antennas and $M_r > 1$ receive antennas, one ULA-IRS with $N > 1$ reflecting elements, and one target at the NLoS region of the AP (i.e., the LoS link between the AP and the target

(a) Point target case
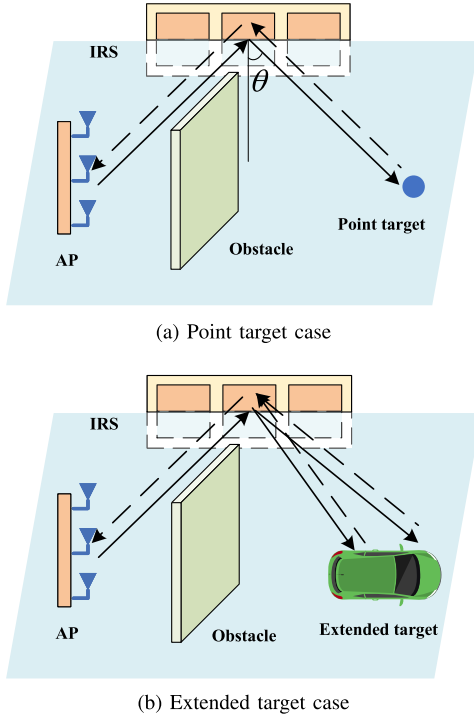

(b) Extended target case

Fig. 1.   System model of IRS-enabled sensing.

is blocked by obstacles such as buildings and trees). We assume the target estimation is implemented at the AP instead of the IRS, as the IRS is often a passive device without the capability of signal processing. In the IRS-enabled sensing system, the AP first optimizes the joint beamforming at the AP and the IRS, and then configures the reflecting elements at the IRS through a smart controller at the IRS [6], [7], [8]. Then, the AP transmits radio signals over the radar dwell time of T and receives the echo signals through the AP-IRS-target-IRS-AP link. After collecting the echo signals over duration time T, the AP processes the signals for target estimation.

First, we consider the transmit and reflective beamforming at the AP and the IRS, respectively. Let $\mathbf{x}(t)$ denote the transmitted signal by the AP at time slot t. The sample covariance matrix of the transmitted signal is

$$\mathbf{R}_x = \frac{1}{T} \sum_{t=1}^{T} \mathbf{x}(t)\mathbf{x}(t)^H, \qquad (1)$$

which corresponds to the transmit beamforming vectors to be optimized. Suppose that $\text{rank}(\mathbf{R}_x) = k$ and the eigenvalue decomposition (EVD) of $\mathbf{R}_x$ is given by

$$\mathbf{R}_x = \mathbf{W}\boldsymbol{\Lambda}\mathbf{W}^H, \qquad (2)$$

where $\boldsymbol{\Lambda} = \text{diag}(\lambda_1, \ldots, \lambda_M)$ and $\mathbf{W} = [\mathbf{w}_1, \ldots, \mathbf{w}_{M_t}]$, with $\lambda_1 \geq \ldots \geq \lambda_k > \lambda_{k+1} = \ldots = \lambda_{M_t} = 0$ and $\mathbf{W}\mathbf{W}^H = \mathbf{W}^H\mathbf{W} = \mathbf{I}_{M_t}$. This means that there are a number of k sensing beams transmitted by the AP, each of which is denoted by $\sqrt{\lambda_i}\mathbf{w}_i, i \in \{1, \ldots, k\}$ (see, e.g., [25]). As for the reflective beamforming, we consider that the IRS can only adjust the phase shifts of its reflecting elements [5]. Let $\mathbf{v} = [e^{j\phi_1}, \ldots, e^{j\phi_N}]^T$ and $\boldsymbol{\Phi} = \text{diag}(\mathbf{v})$ denote the reflective beamforming vector and the corresponding reflection matrix at the IRS, respectively, with

$\phi_n \in (0, 2\pi]$ being the phase shift of element $n \in \{1, \ldots, N\}$, which are optimized later to enhance the sensing performance.

Next, we introduce the channel models. We consider general narrowband channel models for the AP-IRS and IRS-AP links. Let $\mathbf{G}_t \in \mathbb{C}^{N \times M_t}$ and $\mathbf{G}_r \in \mathbb{C}^{M_r \times N}$ denote the channel matrices of the AP-IRS and IRS-AP links, respectively. For the monostatic multiple-input multiple-output (MIMO) radar with $M_t = M_r$, we have $\mathbf{G}_r = \mathbf{G}_t^T$ in general [18], [26]. Let $\mathbf{H}$ denote the target response matrix w.r.t. the IRS (or equivalently the cascaded IRS-target-IRS channel), which can be expressed in the following by considering two specific target models.

1) Point Target Model: When the spatial extent of the target is small, the incident signal is reflected by the target from a singular scatterer [20], [22]. The target response matrix w.r.t. the IRS is modeled as

$$\mathbf{H} = \alpha\mathbf{a}(\theta)\mathbf{a}^T(\theta), \qquad (3)$$

where $\alpha \in \mathbb{C}$ denotes the complex-valued channel coefficient dependent on the target's radar cross section (RCS) and the round-trip path loss of the IRS-target-IRS link, and $\mathbf{a}(\theta)$ denotes the steering vector at the IRS with angle θ, i.e.,

$$\mathbf{a}(\theta) = \left[1, e^{j2\pi \frac{d_{\text{IRS}} \sin\theta}{\lambda_{\text{R}}}}, \ldots, e^{j2\pi \frac{(N-1)d_{\text{IRS}} \sin\theta}{\lambda_{\text{R}}}}\right]^T, \qquad (4)$$

with θ denotes the target's DoA w.r.t. the IRS. In (4), d_{IRS} denotes the spacing between consecutive reflecting elements at the IRS, and λ_{R} denotes the carrier wavelength. In this case, the target's DoA θ is the unknown parameter to be estimated by the AP.

2) Extended Target Model: When the spatial extent of the target is large, the echo signals reflected by the target come from several scatterers in an extended region of space [20], [22], [23], [24]. In this case, the point target model does not accurately reflect the behavior of distributed point-like scatterers, as the echo signals reflected by the extended target consist of multiple signal paths from scatterers with different angles. It is assumed that the AP has no prior knowledge about the distribution of the scatterers. As a result, the AP needs to estimate the complete target response matrix $\mathbf{H}$, such that the angles of scatterers can be recovered from the estimation of the target response matrix using techniques such as the MUSIC algorithm [27], [28], [29].

We now introduce the received signal by the AP, based on the signal propagation procedure detailed in the following.

- First, the AP transmits radio signal $\mathbf{x}(t)$ towards the IRS through the AP-IRS link. The impinged signal at the IRS through the AP-IRS link is $\mathbf{G}_t\mathbf{x}(t)$.
- Next, the IRS reflects the incident signal with reflection matrix $\boldsymbol{\Phi}$, and the departed signal from the IRS is $\boldsymbol{\Phi}\mathbf{G}_t\mathbf{x}(t)$.
- Then, the radio signal illuminates the target. After target reflection (through the AP-IRS-target-IRS link), the impinged signal at the IRS is $\mathbf{H}\boldsymbol{\Phi}\mathbf{G}_t\mathbf{x}(t)$, which is reflected by the IRS again. The departed echo signal from the IRS is $\boldsymbol{\Phi}^T\mathbf{H}\boldsymbol{\Phi}\mathbf{G}_t\mathbf{x}(t)$.
- Finally, by passing through the IRS-AP channel $\mathbf{G}_r$, the echo signal at the AP becomes $\mathbf{G}_r\boldsymbol{\Phi}^T\mathbf{H}\boldsymbol{\Phi}\mathbf{G}_t\mathbf{x}(t)$. By adding noise $\mathbf{n}(t) \sim \mathcal{CN}(\mathbf{0}, \sigma_{\text{R}}^2\mathbf{I}_{M_r})$ at the AP receiver, we have the received signal at time $t \in \{1, \ldots, T\}$:

$$\mathbf{y}(t) = \mathbf{G}_r\boldsymbol{\Phi}^T\mathbf{H}\boldsymbol{\Phi}\mathbf{G}_t\mathbf{x}(t) + \mathbf{n}(t). \qquad (5)$$

Notice that $\mathbf{n}(t)$ may include the background and clutter interference.

We stack the transmitted signals, the received signals, and the noise over the radar dwell time as $\mathbf{X} = [\mathbf{x}(1), \ldots, \mathbf{x}(T)]$, $\mathbf{Y} = [\mathbf{y}(1), \ldots, \mathbf{y}(T)]$, and $\mathbf{N} = [\mathbf{n}(1), \ldots, \mathbf{n}(T)]$, respectively. Accordingly, we have

$$\mathbf{Y} = \mathbf{G}_r \mathbf{\Phi}^T \mathbf{H} \mathbf{\Phi} \mathbf{G}_t \mathbf{X} + \mathbf{N}. \qquad (6)$$

Based on the received echo signal in (6), our objective is to estimate the target's DoA θ in the point target case, and to estimate the target response matrix $\mathbf{H}$ in the extended target case. It is assumed that the AP perfectly knows the CSI $\mathbf{G}_t$ and $\mathbf{G}_r$ of the AP-IRS and IRS-AP links via proper channel estimation algorithms (see, e.g., [30]). This assumption is practically valid, due to the fact that the AP and the IRS are deployed at fixed locations and thus their channels are slowly varying in practice. It is also assumed that the AP perfectly knows its transmitted signal $\mathbf{X}$ (and the associated sample covariance matrix $\mathbf{R}_x$) and the IRS's reflective beamforming vector $\mathbf{v}$ (or $\mathbf{\Phi}$), which can be optimized to enhance the sensing performance.

In the following, Section III obtains the closed-form CRB expressions for target parameters estimation. Sections IV minimize the CRB in (16) or (19) by jointly optimizing the sample covariance matrix $\mathbf{R}_x$ at the AP and the reflective beamforming vector $\mathbf{v}$ at the IRS for the point target case. Sections V minimize the CRB in (26) by optimizing the sample covariance matrix $\mathbf{R}_x$ at the AP for the extended target case.

III. ESTIMATION CRB

This section analyzes the CRB performance in the IRS-enabled NLoS wireless sensing system for the point and extended target cases, respectively.

A. Point Target Case

First, we consider the point target case and derive CRB for estimating the DoA θ. Substituting the target response matrix $\mathbf{H} = \alpha \mathbf{a}(\theta) \mathbf{a}^T(\theta)$ into the received echo signal in (6), we have

$$\mathbf{Y} = \mathbf{G}_r \mathbf{\Phi}^T \alpha \mathbf{a}(\theta) \mathbf{a}^T(\theta) \mathbf{\Phi} \mathbf{G}_t \mathbf{X} + \mathbf{N}. \qquad (7)$$

Let $\boldsymbol{\xi} = [\theta, \tilde{\boldsymbol{\alpha}}^T]^T \in \mathbb{R}^{3 \times 1}$ denote the vector of unknown parameters to be estimated, including the target's DoA θ and the complex-valued channel coefficient α, where $\tilde{\boldsymbol{\alpha}} = [\text{Re}\{\alpha\}, \text{Im}\{\alpha\}]^T$. We are particularly interested in characterizing the CRB for estimating the target's DoA θ. This is due to the fact that it is difficult to extract the target information from the channel coefficient α, as it depends on both the target's RCS and the distance-dependent path loss of the IRS-target-IRS link that are usually unknown.

First, we obtain the Fisher information matrix (FIM) for estimating $\boldsymbol{\xi}$ to facilitate the derivation of the CRB for DoA estimation. Let $\mathbf{B}(\theta) = \mathbf{c}(\theta)\mathbf{b}(\theta)^T$ with $\mathbf{b}(\theta) = \mathbf{G}_t^T \mathbf{\Phi}^T \mathbf{a}(\theta)$ and $\mathbf{c}(\theta) = \mathbf{G}_r \mathbf{\Phi}^T \mathbf{a}(\theta)$, the received echo signal in (7) can be rewritten as

$$\mathbf{Y} = \alpha \mathbf{B}(\theta) \mathbf{X} + \mathbf{N}. \qquad (8)$$

For notational convenience, in the sequel we drop θ in $\mathbf{a}(\theta)$, $\mathbf{b}(\theta)$, $\mathbf{c}(\theta)$, and $\mathbf{B}(\theta)$, and accordingly denote them as $\mathbf{a}$, $\mathbf{b}$, $\mathbf{c}$, and $\mathbf{B}$, respectively. By vectorizing (8), we have

$$\tilde{\mathbf{y}} = \text{vec}(\mathbf{Y}) = \tilde{\mathbf{u}} + \tilde{\mathbf{n}}, \qquad (9)$$

where $\tilde{\mathbf{u}} = \alpha \text{vec}(\mathbf{B}\mathbf{X})$ and $\tilde{\mathbf{n}} = \text{vec}(\mathbf{N}) \sim \mathcal{CN}(\mathbf{0}, \mathbf{R}_n)$ with $\mathbf{R}_n = \sigma_\text{R}^2 \mathbf{I}_{M_r T}$. Let $\tilde{\mathbf{F}} \in \mathbb{R}^{3 \times 3}$ denote the FIM for estimating

$\boldsymbol{\xi}$ based on (9). Since $\tilde{\mathbf{n}} \sim \mathcal{CN}(\mathbf{0}, \sigma_\text{R}^2 \mathbf{I}_{M_r T})$, each element of $\tilde{\mathbf{F}}$ is given by [17]

$$\tilde{\mathbf{F}}_{i,j} = \text{tr}\left(\mathbf{R}_n^{-1} \frac{\partial \mathbf{R}_n}{\partial \boldsymbol{\xi}_i} \mathbf{R}_n^{-1} \frac{\partial \mathbf{R}_n}{\partial \boldsymbol{\xi}_j} \right)$$
$$+ 2\text{Re}\left\{ \frac{\partial \tilde{\mathbf{u}}^H}{\partial \boldsymbol{\xi}_i} \mathbf{R}_n^{-1} \frac{\partial \tilde{\mathbf{u}}}{\partial \boldsymbol{\xi}_j} \right\}, i,j \in \{1,2,3\}. \quad (10)$$

Based on (10), the FIM $\tilde{\mathbf{F}}$ is partitioned as

$$\tilde{\mathbf{F}} = \begin{bmatrix} \tilde{\mathbf{F}}_{\theta\theta} & \tilde{\mathbf{F}}_{\theta\tilde{\alpha}} \\ \tilde{\mathbf{F}}_{\theta\tilde{\alpha}}^T & \tilde{\mathbf{F}}_{\tilde{\alpha}\tilde{\alpha}} \end{bmatrix}, \qquad (11)$$

where

$$\tilde{\mathbf{F}}_{\theta\theta} = \frac{2T|\alpha|^2}{\sigma_\text{R}^2} \text{tr}(\dot{\mathbf{B}} \mathbf{R}_x \dot{\mathbf{B}}^H), \qquad (12)$$

$$\tilde{\mathbf{F}}_{\theta\tilde{\alpha}} = \frac{2T}{\sigma_\text{R}^2} \text{Re}\{\alpha^* \text{tr}(\mathbf{B} \mathbf{R}_x \dot{\mathbf{B}}^H)[1,j]\}, \qquad (13)$$

$$\tilde{\mathbf{F}}_{\tilde{\alpha}\tilde{\alpha}} = \frac{2T}{\sigma_\text{R}^2} \text{tr}(\mathbf{B} \mathbf{R}_x \mathbf{B}^H) \mathbf{I}_2, \qquad (14)$$

with $j = \sqrt{-1}$ and $\dot{\mathbf{B}} = \frac{\partial \mathbf{B}}{\partial \theta}$ denoting the partial derivative of $\mathbf{B}$ w.r.t. θ. The derivation of the FIM $\tilde{\mathbf{F}}$ follows the standard procedure in [18]; see details in Appendix A.

Next, we derive the CRB for estimating the DoA, which corresponds to the first diagonal element of $\tilde{\mathbf{F}}^{-1}$, i.e.,

$$\text{CRB}(\theta) = [\tilde{\mathbf{F}}^{-1}]_{1,1} = [\tilde{\mathbf{F}}_{\theta\theta} - \tilde{\mathbf{F}}_{\theta\tilde{\alpha}} \tilde{\mathbf{F}}_{\tilde{\alpha}\tilde{\alpha}}^{-1} \tilde{\mathbf{F}}_{\theta\tilde{\alpha}}^T]^{-1}. \quad (15)$$

Based on (15) and (11), we have the following lemma.
Lemma 1: The CRB for estimating the DoA θ is given by

$$\text{CRB}(\theta) = \frac{\sigma_\text{R}^2}{2T|\alpha|^2 \left(\text{tr}(\dot{\mathbf{B}} \mathbf{R}_x \dot{\mathbf{B}}^H) - \frac{|\text{tr}(\mathbf{B} \mathbf{R}_x \dot{\mathbf{B}}^H)|^2}{\text{tr}(\mathbf{B} \mathbf{R}_x \mathbf{B}^H)} \right)}. \quad (16)$$

To gain more insight and facilitate the reflective beamforming design, we re-express $\text{CRB}(\theta)$ in (16) w.r.t. the reflective beamforming vector $\mathbf{v}$. Towards this end, we introduce $\mathbf{A} = \text{diag}(\mathbf{a})$, and accordingly have $\mathbf{b} = \mathbf{G}_t^T \mathbf{\Phi}^T \mathbf{a} = \mathbf{G}_t^T \mathbf{A} \mathbf{v}$ and $\mathbf{c} = \mathbf{G}_r \mathbf{\Phi}^T \mathbf{a} = \mathbf{G}_r \mathbf{A} \mathbf{v}$. Let $\dot{\mathbf{b}}$ and $\dot{\mathbf{c}}$ and denote the partial derivative of $\mathbf{b}$ and $\mathbf{c}$ w.r.t. θ, respectively, where $\dot{\mathbf{b}} = j2\pi \frac{d_\text{IRS}}{\lambda_\text{R}} \cos\theta \mathbf{G}_t^T \mathbf{\Phi}^T \mathbf{D} \mathbf{a} = j2\pi \frac{d_\text{IRS}}{\lambda_\text{R}} \cos\theta \mathbf{G}_t^T \mathbf{A} \mathbf{D} \mathbf{v}$ and $\dot{\mathbf{c}} = j2\pi \frac{d_\text{IRS}}{\lambda_\text{R}} \cos\theta \mathbf{G}_r \mathbf{\Phi}^T \mathbf{D} \mathbf{a} = j2\pi \frac{d_\text{IRS}}{\lambda_\text{R}} \cos\theta \mathbf{G}_r \mathbf{A} \mathbf{D} \mathbf{v}$ with $\mathbf{D} = \text{diag}(0,1,\ldots,N-1)$. As a result,

$$\mathbf{B} = \mathbf{c} \mathbf{b}^T = \mathbf{G}_r \mathbf{A} \mathbf{v} \mathbf{v}^T \mathbf{A}^T \mathbf{G}_t^T, \qquad (17)$$

$$\dot{\mathbf{B}} = \dot{\mathbf{c}} \mathbf{b}^T + \mathbf{c} \dot{\mathbf{b}}^T.$$

$$= j2\pi \frac{d_\text{IRS}}{\lambda_\text{R}} \cos\theta \mathbf{G}_r \mathbf{A} (\mathbf{D} \mathbf{v} \mathbf{v}^T + \mathbf{v} \mathbf{v}^T \mathbf{D}^T) \mathbf{A}^T \mathbf{G}_t. \quad (18)$$

Then we have the following lemma.

Lemma 2: The CRB for estimating the DoA θ, i.e., $\mathrm{CRB}(\theta)$ in (16), can be re-expressed in (19) shown at the bottom of this page, w.r.t. $\mathbf{v}$, where $\mathbf{R}_1 = \mathbf{A}^H \mathbf{G}_r^H \mathbf{G}_r \mathbf{A}$ and $\mathbf{R}_2 = \mathbf{A}^H \mathbf{G}_t^* \mathbf{R}_x^* \mathbf{G}_t^T \mathbf{A}$.

Proof: This lemma is verified by substituting (17) and (18) into (16). ∎

Based on $\mathrm{CRB}(\theta)$ in (19), we have the following proposition.

Proposition 1: If $\mathrm{rank}(\mathbf{G}_t) = \mathrm{rank}(\mathbf{G}_r) = 1$ (or equivalently there is only one single path between the AP and the IRS), then the FIM $\tilde{\mathbf{F}}$ in (10) for estimating $\boldsymbol{\xi}$ is a singular matrix, and $\mathrm{CRB}(\theta) = \infty$. Otherwise, the FIM $\tilde{\mathbf{F}}$ is invertible, and $\mathrm{CRB}(\theta)$ is bounded.

Proof: See Appendix B. ∎

Proposition 1 shows that the target's DoA θ can only be estimated only when $\mathrm{rank}(\mathbf{G}_t) > 1$ or $\mathrm{rank}(\mathbf{G}_r) > 1$ (i.e., the number of signal paths between the AP and the IRS is larger than one). The reasons are intuitively explained as follows. When $\mathrm{rank}(\mathbf{G}_t) = \mathrm{rank}(\mathbf{G}_r) = 1$, the truncated SVD of $\mathbf{G}_t$ and $\mathbf{G}_t$ are expressed as $\mathbf{G}_t = \sigma_{1,t} \mathbf{s}_{1,t} \mathbf{q}_{1,t}^T$ and $\mathbf{G}_r = \sigma_{1,r} \mathbf{s}_{1,r} \mathbf{q}_{1,r}^T$, where $\mathbf{s}_{1,t}, \mathbf{s}_{1,r}$ and $\mathbf{q}_{1,t}, \mathbf{q}_{1,r}$ are the left and right dominant singular vectors, and $\sigma_{1,t}, \sigma_{1,r}$ are the dominant singular values of the corresponding matrices. Accordingly, the received echo signal in (5) at the AP is given by

$$\mathbf{y}(t) = \alpha \sigma_{1,t} \sigma_{1,r} \mathbf{s}_{1,r} \underbrace{\mathbf{q}_{1,r}^T \boldsymbol{\Phi}^T \mathbf{a} \mathbf{a}^T \boldsymbol{\Phi} \mathbf{s}_{1,t}}_{\beta(\theta)} \underbrace{\mathbf{q}_{1,t}^T \mathbf{x}(t)}_{\tilde{x}(t)} + \mathbf{n}(t), \quad (20)$$

where $\beta(\theta) = \mathbf{q}_{1,r}^T \boldsymbol{\Phi}^T \mathbf{a} \mathbf{a}^T \boldsymbol{\Phi} \mathbf{s}_{1,t}$ is the only term related to θ. Notice that in (20), the complex numbers α and $\beta(\theta)$ are coupled. Therefore, from $\mathbf{y}(t)$, we can only recover one observation on $\alpha \beta(\theta)$, which is not sufficient to extract $\beta(\theta)$, thus making the DoA θ is not estimated.[1]

B. Extended Target Case

This subsection derives the CRB for estimating the target response matrix $\mathbf{H}$. For the extended target case, the AP aims to estimate the whole target response matrix $\mathbf{H}$ by processing the received echo signal in (6), which is a linear estimation problem with Gaussian noise w.r.t $\mathbf{H}$ and hence the CRB does not depend on the ground truth of $\mathbf{H}$. Let $\boldsymbol{\zeta} = [\mathbf{h}_R^T, \mathbf{h}_I^T]^T \in \mathbb{R}^{2N^2 \times 1}$ denote the vector of unknown parameters to be estimated, where $\mathbf{h}_R = \mathrm{Re}(\mathbf{h})$ and $\mathbf{h}_I = \mathrm{Im}(\mathbf{h})$ are the real and imaginary parts of $\mathbf{h} = \mathrm{vec}(\mathbf{H})$, respectively.

First, we obtain the FIM for estimating the target response matrix $\mathbf{H}$. Similarly as in (9), for the extended target case, the received echo signal is rewritten as

$$\hat{\mathbf{y}} = \mathrm{vec}(\mathbf{Y}) = \hat{\mathbf{u}} + \hat{\mathbf{n}}, \quad (21)$$

where $\hat{\mathbf{u}} = \mathrm{vec}(\mathbf{G}_r \boldsymbol{\Phi}^T \mathbf{H} \boldsymbol{\Phi} \mathbf{G}_t \mathbf{X}) = (\mathbf{X}^T \mathbf{G}_t^T \boldsymbol{\Phi}^T \otimes \mathbf{G}_r \boldsymbol{\Phi}^T) \mathbf{h}$ and $\hat{\mathbf{n}} = \mathrm{vec}(\mathbf{N}) \sim \mathcal{CN}(\mathbf{0}, \mathbf{R}_n)$ with $\mathbf{R}_n = \sigma_R^2 \mathbf{I}_{M_r T}$. Let $\hat{\mathbf{F}} \in \mathbb{R}^{2N^2 \times 2N^2}$ denote the FIM for estimating $\boldsymbol{\zeta}$ based on (21). As

---

[1]When $\mathrm{rank}(\mathbf{G}_t) = \mathrm{rank}(\mathbf{G}_r) = 1$, we can use detection methods based on, e.g., generalized likelihood ratio test [13] and beam scanning [9] to detect the existence of a target based on observation of the product $\alpha \beta(\theta)$. However, these methods cannot accurately estimate the target angle θ, as shown in Proposition 1.

in (10), each element of $\hat{\mathbf{F}}$ is given by

$$\hat{\mathbf{F}}_{i,j} = \mathrm{tr}\left(\mathbf{R}_n^{-1} \frac{\partial \mathbf{R}_n}{\partial \zeta_i} \mathbf{R}_n^{-1} \frac{\partial \mathbf{R}_n}{\partial \zeta_j}\right)$$
$$+ 2\mathrm{Re}\left\{\frac{\partial \hat{\mathbf{u}}^H}{\partial \zeta_i} \mathbf{R}_n^{-1} \frac{\partial \hat{\mathbf{u}}}{\partial \zeta_j}\right\}, i, j \in \{1, \ldots, 2N^2\}. \quad (22)$$

Based on (22), the FIM $\hat{\mathbf{F}}$ is partitioned as

$$\hat{\mathbf{F}} = \begin{bmatrix} \hat{\mathbf{F}}_{\mathbf{h}_R \mathbf{h}_R} & \hat{\mathbf{F}}_{\mathbf{h}_R \mathbf{h}_I} \\ \hat{\mathbf{F}}_{\mathbf{h}_I \mathbf{h}_R} & \hat{\mathbf{F}}_{\mathbf{h}_I \mathbf{h}_I} \end{bmatrix}, \quad (23)$$

where

$$\hat{\mathbf{F}}_{\mathbf{h}_R \mathbf{h}_R} = \hat{\mathbf{F}}_{\mathbf{h}_I \mathbf{h}_I}$$
$$= \frac{2T}{\sigma_R^2} \mathrm{Re}\{(\boldsymbol{\Phi}^* \mathbf{G}_t^* \mathbf{R}_x^T \mathbf{G}_t^T \boldsymbol{\Phi}^T) \otimes (\boldsymbol{\Phi}^* \mathbf{G}_r^H \mathbf{G}_r \boldsymbol{\Phi}^T)\}, \quad (24)$$

$$\hat{\mathbf{F}}_{\mathbf{h}_I \mathbf{h}_R} = -\hat{\mathbf{F}}_{\mathbf{h}_R \mathbf{h}_I}$$
$$= \frac{2T}{\sigma_R^2} \mathrm{Im}\{(\boldsymbol{\Phi}^* \mathbf{G}_t^* \mathbf{R}_x^T \mathbf{G}_t^T \boldsymbol{\Phi}^T) \otimes (\boldsymbol{\Phi}^* \mathbf{G}_r^H \mathbf{G}_r \boldsymbol{\Phi}^T)\}. \quad (25)$$

The detailed derivations are shown in Appendix C. Based on (23), the CRB for estimating $\mathbf{H}$ is obtained in the following lemma.

Lemma 3: The CRB for estimating the target response matrix $\mathbf{H}$ is given by

$$\mathrm{CRB}(\mathbf{H}) = \frac{\sigma_R^2}{T} \mathrm{tr}((\mathbf{G}_t \mathbf{R}_x \mathbf{G}_t^H)^{-1}) \mathrm{tr}((\mathbf{G}_r^H \mathbf{G}_r)^{-1}). \quad (26)$$

Proof: It follows from (23) that

$$\mathrm{CRB}(\mathbf{H}) = \mathrm{CRB}(\boldsymbol{\zeta}) = \mathrm{tr}(\hat{\mathbf{F}}^{-1})$$
$$= \frac{\sigma_R^2}{T} \mathrm{tr}((\boldsymbol{\Phi} \mathbf{G}_t \mathbf{R}_x \mathbf{G}_t^H \boldsymbol{\Phi}^H)^{-1}) \mathrm{tr}((\boldsymbol{\Phi} \mathbf{G}_r^T \mathbf{G}_r^* \boldsymbol{\Phi}^H)^{-1})$$
$$= \frac{\sigma_R^2}{T} \mathrm{tr}(\boldsymbol{\Phi}^H (\mathbf{G}_t \mathbf{R}_x \mathbf{G}_t^H)^{-1} \boldsymbol{\Phi}) \mathrm{tr}(\boldsymbol{\Phi}^H (\mathbf{G}_r^T \mathbf{G}_r^*)^{-1} \boldsymbol{\Phi})$$
$$= \frac{\sigma_R^2}{T} \mathrm{tr}((\mathbf{G}_t \mathbf{R}_x \mathbf{G}_t^H)^{-1}) \mathrm{tr}((\mathbf{G}_r^H \mathbf{G}_r)^{-1}), \quad (27)$$

completing the proof. ∎

It is observed from Lemma 3 that $\mathrm{CRB}(\mathbf{H})$ in the extended target case only depends on the transmit beamformers or the sample covariance matrix $\mathbf{R}_x$, regardless of the reflective beamformer $\boldsymbol{\Phi}$. This can be intuitively explained by introducing $\hat{\mathbf{H}} = \boldsymbol{\Phi}^T \mathbf{H} \boldsymbol{\Phi}$ as the equivalent target response matrix by taking into account the reflective beamformer at the IRS. In this case, the received echo signal in (6) is rewritten as

$$\mathbf{Y} = \mathbf{G}_r \hat{\mathbf{H}} \mathbf{G}_t \mathbf{X} + \mathbf{N}. \quad (28)$$

Note that, (28) is a linear white Gaussian model w.r.t $\hat{\mathbf{H}}$ and hence the CRB for estimating $\hat{\mathbf{H}}$ does not depend on the ground truth of $\hat{\mathbf{H}}$, thus does not depend on the reflective beamformer $\boldsymbol{\Phi}$. On the other hand, as $\boldsymbol{\Phi}$ is a full-rank diagonal matrix with unit-modulus constraint on each element, we can always recover $\mathbf{H}$

$$\mathrm{CRB}(\theta) = \frac{\sigma_R^2 \lambda_R^2}{8T |\alpha|^2 \pi^2 d_{\mathrm{IRS}}^2 \cos^2(\theta) \left(\mathbf{v}^H \mathbf{R}_2 \mathbf{v} \left(\mathbf{v}^H \mathbf{D} \mathbf{R}_1 \mathbf{D} \mathbf{v} - \frac{|\mathbf{v}^H \mathbf{D} \mathbf{R}_1 \mathbf{v}|^2}{\mathbf{v}^H \mathbf{R}_1 \mathbf{v}}\right) + \mathbf{v}^H \mathbf{R}_1 \mathbf{v} \left(\mathbf{v}^H \mathbf{D} \mathbf{R}_2 \mathbf{D} \mathbf{v} - \frac{|\mathbf{v}^H \mathbf{D} \mathbf{R}_2 \mathbf{v}|^2}{\mathbf{v}^H \mathbf{R}_2 \mathbf{v}}\right)\right)} \quad (19)$$

from $\hat{\mathbf{H}}$ based on $\mathbf{H} = \mathbf{\Phi}^*\hat{\mathbf{H}}\mathbf{\Phi}^H$ without losing any information, i.e., the CRB for estimating $\mathbf{H}$ is identical to that of $\hat{\mathbf{H}}$. By combining the two facts, the result in Lemma 3 that $\text{CRB}(\mathbf{H})$ is independent of $\mathbf{\Phi}$ is evident.

Based on the FIM $\hat{\mathbf{F}}$ in (23) and $\text{CRB}(\mathbf{H})$ in (26), we have the following proposition.

Proposition 2: If $\text{rank}(\mathbf{G}_t) < N$ or $\text{rank}(\mathbf{G}_r) < N$, then the FIM $\hat{\mathbf{F}}$ in (23) for estimating $\mathbf{H}$ is a singular matrix, and $\text{CRB}(\mathbf{H}) = \infty$. Otherwise, the FIM $\hat{\mathbf{F}}$ is invertible, and $\text{CRB}(\mathbf{H})$ is bounded.

Proposition 2 shows that the target response matrix $\mathbf{H}$ can only be estimated only when[2] $\text{rank}(\mathbf{G}_t) = \text{rank}(\mathbf{G}_r) = N$.

IV. JOINT BEAMFORMING OPTIMIZATION FOR CRB MINIMIZATION WITH POINT TARGET

In this section, we propose to jointly optimize the transmit beamforming at the AP and the reflective beamforming at the IRS to minimize the CRB for estimating the DoA in (16) or (19) in the point target case, subject to a maximum transmit power constraint at the AP. Note that in order to implement the joint beamforming design, we assume that the AP roughly knows the information of θ, which corresponds to the target tracking scenario in practice. Also note that the AP does not need to know the channel coefficient α, as it is independent of the joint beamforming design. The CRB minimization problem is formulated as

$$(\text{P1}): \min_{\mathbf{R}_x, \mathbf{v}} \quad \text{CRB}(\theta)$$

$$\text{s.t.} \quad \text{tr}(\mathbf{R}_x) \leq P_0 \quad (29\text{a})$$

$$\mathbf{R}_x \succeq \mathbf{0} \quad (29\text{b})$$

$$\mathbf{\Phi} = \text{diag}(\mathbf{v}) \quad (29\text{c})$$

$$|\mathbf{v}_n| = 1, \forall n \in \{1, \ldots, N\}, \quad (29\text{d})$$

where P_0 is the maximum transmit power at the AP.

Problem (P1) is difficult to solve due to the non-convexity of the objective function, the unit-modulus constraint in (29d), and the coupled relationship between the transmit and reflective beamformers. In order to solve the non-convex problem (P1) efficiently, we use an alternating optimization technique by decomposing (P1) into two subproblems and iteratively solving them in an alternating manner. For each subproblem, we use various optimization techniques such as SCA and SDR.

A. Transmit Beamforming Optimization

First, we optimize the transmit beamformers $\mathbf{R}_x$ in problem (P1) under any given reflective beamformer $\mathbf{v}$, in which the CRB formula in (16) is used. In this case, minimizing $\text{CRB}(\theta)$ is equivalent to maximizing $\text{tr}(\dot{\mathbf{B}}\mathbf{R}_x\dot{\mathbf{B}}^H) - \frac{|\text{tr}(\mathbf{B}\mathbf{R}_x\dot{\mathbf{B}}^H)|^2}{\text{tr}(\mathbf{B}\mathbf{R}_x\mathbf{B}^H)}$. As a result, the transmit beamforming optimization problem is

[2]It is worth noting that if $\text{rank}(\mathbf{G}_t) < N$ or $\text{rank}(\mathbf{G}_r) < N$ for the extended target case, then the FIM for estimating the target response matrix $\mathbf{H}$ becomes singular. As a result, the corresponding CRB is infinite, i.e., there is no unbiased estimator with finite variance for estimating $\mathbf{H}$. As an initial work on IRS-enabled sensing, in this article we only focus on the case with $\text{rank}(\mathbf{G}_t) = \text{rank}(\mathbf{G}_r) = N$, while our proposed designs are generally extendable to the case with $\text{rank}(\mathbf{G}_t) < N$ or $\text{rank}(\mathbf{G}_r) < N$.

formulated as

$$(\text{P2}): \max_{\mathbf{R}_x} \quad \text{tr}(\dot{\mathbf{B}}\mathbf{R}_x\dot{\mathbf{B}}^H) - \frac{|\text{tr}(\mathbf{B}\mathbf{R}_x\dot{\mathbf{B}}^H)|^2}{\text{tr}(\mathbf{B}\mathbf{R}_x\mathbf{B}^H)}$$

$$\text{s.t.} \quad (29\text{a}) \text{ and } (29\text{b}).$$

By introducing an auxiliary variable t, problem (P2) is equivalently re-expressed as

$$(\text{P2.1}): \max_{\mathbf{R}_x, t} \quad t$$

$$\text{s.t.} \quad \text{tr}(\dot{\mathbf{B}}\mathbf{R}_x\dot{\mathbf{B}}^H) - \frac{|\text{tr}(\mathbf{B}\mathbf{R}_x\dot{\mathbf{B}}^H)|^2}{\text{tr}(\mathbf{B}\mathbf{R}_x\mathbf{B}^H)} \geq t$$

$$(29\text{a}) \text{ and } (29\text{b}). \quad (30\text{a})$$

Using Schur's complement [31], the constraint in (30a) is equivalently transformed into the following convex semi-definite constraint:

$$\begin{bmatrix} \text{tr}(\dot{\mathbf{B}}\mathbf{R}_x\dot{\mathbf{B}}^H) - t & \text{tr}(\mathbf{B}\mathbf{R}_x\dot{\mathbf{B}}^H) \\ \text{tr}(\dot{\mathbf{B}}\mathbf{R}_x\mathbf{B}^H) & \text{tr}(\mathbf{B}\mathbf{R}_x\mathbf{B}^H) \end{bmatrix} \succeq \mathbf{0}. \quad (31)$$

Accordingly, problem (P2.1) is equivalent to the following semi-definite program (SDP), which can be optimally solved by convex solvers such as CVX [32]:

$$(\text{P2.2}): \max_{\mathbf{R}_x, t} \quad t$$

$$\text{s.t.} \quad (29\text{a}), (29\text{b}), \text{ and } (31).$$

B. Reflective Beamforming Optimization

Next, we optimize the reflecting beamformer $\mathbf{v}$ in problem (P1) under any given transmit beamformers $\mathbf{R}_x$, in which the CRB formula in (19) is used. In this case, the reflective beamforming optimization problem is formulated as

$$(\text{P3}): \max_{\mathbf{v}} \quad \mathbf{v}^H\mathbf{R}_2\mathbf{v}\left(\mathbf{v}^H\mathbf{D}\mathbf{R}_1\mathbf{D}\mathbf{v} - \frac{|\mathbf{v}^H\mathbf{D}\mathbf{R}_1\mathbf{v}|^2}{\mathbf{v}^H\mathbf{R}_1\mathbf{v}}\right)$$

$$+ \mathbf{v}^H\mathbf{R}_1\mathbf{v}\left(\mathbf{v}^H\mathbf{D}\mathbf{R}_2\mathbf{D}\mathbf{v} - \frac{|\mathbf{v}^H\mathbf{D}\mathbf{R}_2\mathbf{v}|^2}{\mathbf{v}^H\mathbf{R}_2\mathbf{v}}\right)$$

$$\text{s.t.} \quad (29\text{d}),$$

which is still non-convex due to the non-concavity of the objective function and the unit-modulus constraint in (29d). To resolve this issue, we first deal with constraint (29d) based on SDR, and then use SCA to approximate the relaxed problem.

Define $\mathbf{V} = \mathbf{v}\mathbf{v}^H$ with $\mathbf{V} \succeq \mathbf{0}$ and $\text{rank}(\mathbf{V}) = 1$. Based on (29d), $\mathbf{V}_{n,n} = 1, \forall n \in \{1, \ldots, N\}$. Also, we have $\mathbf{v}^H\mathbf{R}_1\mathbf{v} = \text{tr}(\mathbf{R}_1\mathbf{V})$, $\mathbf{v}^H\mathbf{R}_2\mathbf{v} = \text{tr}(\mathbf{R}_2\mathbf{V})$, $\mathbf{v}^H\mathbf{D}\mathbf{R}_1\mathbf{v} = \text{tr}(\mathbf{D}\mathbf{R}_1\mathbf{V})$, $\mathbf{v}^H\mathbf{D}\mathbf{R}_2\mathbf{v} = \text{tr}(\mathbf{D}\mathbf{R}_2\mathbf{V})$, $\mathbf{v}^H\mathbf{D}\mathbf{R}_1\mathbf{D}\mathbf{v} = \text{tr}(\mathbf{D}\mathbf{R}_1\mathbf{D}\mathbf{V})$, and $\mathbf{v}^H\mathbf{D}\mathbf{R}_2\mathbf{D}\mathbf{v} = \text{tr}(\mathbf{D}\mathbf{R}_2\mathbf{D}\mathbf{V})$.

Note that the only non-convex constraint on $\mathbf{V}$ is the rank-one constraint $\text{rank}(\mathbf{V}) = 1$. By substituting $\mathbf{V} = \mathbf{v}\mathbf{v}^H$ and dropping this rank-one constraint, problem (P3) is approximated as

$$(\text{P3.1}): \max_{\mathbf{V}} \quad \text{tr}(\mathbf{R}_2\mathbf{V})\text{tr}(\mathbf{D}\mathbf{R}_1\mathbf{D}\mathbf{V}) - \text{tr}(\mathbf{R}_2\mathbf{V})\frac{|\text{tr}(\mathbf{D}\mathbf{R}_1\mathbf{V})|^2}{\text{tr}(\mathbf{R}_1\mathbf{V})}$$

$$+ \text{tr}(\mathbf{R}_1\mathbf{V})\text{tr}(\mathbf{D}\mathbf{R}_2\mathbf{D}\mathbf{V}) - \text{tr}(\mathbf{R}_1\mathbf{V})\frac{|\text{tr}(\mathbf{D}\mathbf{R}_2\mathbf{V})|^2}{\text{tr}(\mathbf{R}_2\mathbf{V})}$$

$$\text{s.t. } \mathbf{V}_{n,n} = 1, \forall n \in \{1, 2, \ldots, N\} \tag{32a}$$

$$\mathbf{V} \succeq \mathbf{0}. \tag{32b}$$

Next, we use Schur's complement and SCA to deal with the non-concave objective function. By introducing two auxiliary variables t_1 and t_2 and reformulating the objective function, problem (P3.1) is equivalently re-expressed as

$$(\text{P3.2}): \max_{\mathbf{V}, t_1, t_2} \quad f_1(\mathbf{V}, t_1, t_2) + f_2(\mathbf{V}, t_1, t_2)$$

$$\text{s.t. } t_1 \geq \frac{|\text{tr}(\mathbf{D}\mathbf{R}_1\mathbf{V})|^2}{\text{tr}(\mathbf{R}_1\mathbf{V})} \tag{33a}$$

$$t_2 \geq \frac{|\text{tr}(\mathbf{D}\mathbf{R}_2\mathbf{V})|^2}{\text{tr}(\mathbf{R}_2\mathbf{V})}$$

$$(\text{32a}) \text{ and } (\text{32b}), \tag{33b}$$

where

$$f_1(\mathbf{V}, t_1, t_2)$$
$$= \frac{1}{4}\text{tr}^2((\mathbf{R}_2 + \mathbf{D}\mathbf{R}_1\mathbf{D})\mathbf{V}) + \frac{1}{4}(\text{tr}(\mathbf{R}_2\mathbf{V}) - t_1)^2$$
$$+ \frac{1}{4}\text{tr}^2((\mathbf{R}_1 + \mathbf{D}\mathbf{R}_2\mathbf{D})\mathbf{V}) + \frac{1}{4}(\text{tr}(\mathbf{R}_1\mathbf{V}) - t_2)^2 \tag{34}$$

and

$$f_2(\mathbf{V}, t_1, t_2)$$
$$= -\frac{1}{4}\text{tr}^2((\mathbf{R}_2 - \mathbf{D}\mathbf{R}_1\mathbf{D})\mathbf{V}) - \frac{1}{4}(\text{tr}(\mathbf{R}_2\mathbf{V}) + t_1)^2$$
$$- \frac{1}{4}\text{tr}^2((\mathbf{R}_1 - \mathbf{D}\mathbf{R}_2\mathbf{D})\mathbf{V}) - \frac{1}{4}(\text{tr}(\mathbf{R}_1\mathbf{V}) + t_2)^2. \tag{35}$$

Here, $f_1(\mathbf{V}, t_1, t_2)$ and $f_2(\mathbf{V}, t_1, t_2)$ are convex and concave functions, respectively.

Using Schur's complement, the constraints in (33a) and (33b) are equivalently transformed into the following convex semidefinite constraints:

$$\begin{bmatrix} t_1 & \text{tr}(\mathbf{D}\mathbf{R}_1\mathbf{V}) \\ \text{tr}(\mathbf{V}^H\mathbf{R}_1^H\mathbf{D}^H) & \text{tr}(\mathbf{R}_1\mathbf{V}) \end{bmatrix} \succeq \mathbf{0}, \tag{36}$$

$$\begin{bmatrix} t_2 & \text{tr}(\mathbf{D}\mathbf{R}_2\mathbf{V}) \\ \text{tr}(\mathbf{V}^H\mathbf{R}_2^H\mathbf{D}^H) & \text{tr}(\mathbf{R}_2\mathbf{V}) \end{bmatrix} \succeq \mathbf{0}. \tag{37}$$

Problem (P3.2) is then equivalent to the following problem:

$$(\text{P3.3}): \max_{\mathbf{V}, t_1, t_2} \quad f_1(\mathbf{V}, t_1, t_2) + f_2(\mathbf{V}, t_1, t_2)$$

$$\text{s.t. } (\text{32a}), (\text{32b}), (\text{36}), \text{ and } (\text{37}).$$

Note that in problem (P3.3), all constraints are convex, but $f_1(\mathbf{V}, t_1, t_2)$ in the objective function is non-concave, thus making problem (P3.3) non-convex. We use SCA to deal with the non-concave function $f_1(\mathbf{V}, t_1, t_2)$ for solving the non-convex problem (P3.3), based on which problem (P3.3) is approximated as a series of convex problems. The SCA-based solution is implemented in an iterative manner as follows. Consider inner iteration $r \geq 1$, in which the local point is denoted by $\mathbf{V}^{(r)}$, $t_1^{(r)}$, and $t_2^{(r)}$. Based on the local point, we obtain a global linear lower bound function $\hat{f}_1^{(r)}(\mathbf{V}, t_1, t_2)$ for the convex function $f_1(\mathbf{V}, t_1, t_2)$ in (P3.3), using its first-order Taylor expansion,

i.e.,

$$f_1(\mathbf{V}, t_1, t_2)$$

$$\geq f_1(\mathbf{V}^{(r)}, t_1^{(r)}, t_2^{(r)}) + \frac{1}{2}\text{tr}((\mathbf{R}_2 + \mathbf{D}\mathbf{R}_1\mathbf{D})\mathbf{V}^{(r)})$$

$$\text{tr}((\mathbf{R}_2 + \mathbf{D}\mathbf{R}_1\mathbf{D})(\mathbf{V} - \mathbf{V}^{(r)})) + \frac{1}{2}\text{tr}((\mathbf{R}_1$$

$$+ \mathbf{D}\mathbf{R}_2\mathbf{D})\mathbf{V}^{(r)})\text{tr}((\mathbf{R}_1 + \mathbf{D}\mathbf{R}_2\mathbf{D})(\mathbf{V} - \mathbf{V}^{(r)}))$$

$$+ \frac{1}{2}t_1^{(r)}(t_1 - t_1^{(r)}) + \frac{1}{2}t_2^{(r)}(t_2 - t_2^{(r)})$$

$$+ \frac{1}{2}\text{tr}(\mathbf{R}_2\mathbf{V}^{(r)})\text{tr}(\mathbf{R}_2(\mathbf{V} - \mathbf{V}^{(r)}))$$

$$+ \frac{1}{2}\text{tr}(\mathbf{R}_1\mathbf{V}^{(r)})\text{tr}(\mathbf{R}_1(\mathbf{V} - \mathbf{V}^{(r)}))$$

$$\triangleq \hat{f}_1^{(r)}(\mathbf{V}, t_1, t_2). \tag{38}$$

Replacing $f_1(\mathbf{V}, t_1, t_2)$ by $\hat{f}_1^{(r)}(\mathbf{V}, t_1, t_2)$, problem (P3.3) is approximated as the following convex form in inner iteration r:

$$(\text{P3.3}.r): \max_{\mathbf{V}, t_1, t_2} \quad \hat{f}_1^{(r)}(\mathbf{V}, t_1, t_2) + f_2(\mathbf{V}, t_1, t_2)$$

$$\text{s.t. } (\text{32a}), (\text{32b}), (\text{36}), \text{ and } (\text{37}),$$

which can be optimally solved by convex solvers such as CVX. Let $\hat{\mathbf{V}}^\star$, $\hat{t}_1^\star$, and $\hat{t}_2^\star$ denote the optimal solution to problem (P3.3.r), which is then updated to be the local point $\mathbf{V}^{(r+1)}$, $t_1^{(r+1)}$, and $t_2^{(r+1)}$ for the next inner iteration. Since $\hat{f}_1^{(r)}(\mathbf{V}, t_1, t_2)$ serves as a lower bound of $f_1(\mathbf{V}, t_1, t_2)$, it is ensured that $f_1(\mathbf{V}^{(r+1)}, t_1^{(r+1)}, t_2^{(r+1)}) + f_2(\mathbf{V}^{(r+1)}, t_1^{(r+1)}, t_2^{(r+1)}) \geq f_1(\mathbf{V}^{(r)}, t_1^{(r)}, t_2^{(r)}) + f_2(\mathbf{V}^{(r)}, t_1^{(r)}, t_2^{(r)})$, i.e., the inner iteration leads to a non-decreasing objective value for problem (P3.3). Therefore, the convergence of SCA for solving problem (P3.3) is ensured and a suboptimal solution of problem (P3.3) is obtained. Let $\tilde{\mathbf{V}}$, $\tilde{t}_1$, and $\tilde{t}_2$ denote the obtained solution to problem (P3.3) based on SCA, where $\text{rank}(\tilde{\mathbf{V}}) > 1$ may hold in general.

Finally, we construct an approximate rank-one solution of $\mathbf{V}$ to problem (P3.3) or (P3) by using Gaussian randomization. Specifically, we first generate a number of random realizations $\mathbf{z} \sim \mathcal{CN}(\mathbf{0}, \tilde{\mathbf{V}})$, and construct a set of candidate feasible solutions as

$$\mathbf{v} = e^{j\arg(\mathbf{z})}. \tag{39}$$

We then choose the best $\mathbf{v}$ that achieves the maximum objective value of problem (P3.3) or (P3).

C. Complete Algorithm of Alternating Optimization

By combining Sections IV-A and IV-B, the alternating optimization based algorithm for solving problem (P1) is summarized as Algorithm 1 in Table I. In each outer iteration, we first solve problem (P2) to update the transmit beamformers $\mathbf{R}_x$ with the updated reflective beamformer $\mathbf{v}$ in the previous round, and then solve problem (P3) to update $\mathbf{v}$ with the updated $\mathbf{R}_x$. In each outer iteration of alternating optimization, problem (P2) is optimally solved, thus leading to a non-increasing CRB value. With sufficient number of Gaussian randomizations, the SDR approach achieves at least $\frac{\pi}{4}$-approximation of the optimal

TABLE I
ALGORITHM 1 FOR JOINT TRANSMIT AND REFLECTIVE BEAMFORMING
OPTIMIZATION WITH POINT TARGET

Algorithm 1
a) Set outer iteration index $l = 1$ and initialize the reflective beamformer with random phase shifts as $\mathbf{v}^{(l)}$
b) **Repeat**:
1) Under given reflective beamformer $\mathbf{v}^{(l)}$, solve problem (P2.2) to obtain the optimal solution as $\mathbf{R}_x^{(l)}$
2) Set inner iteration index $r = 1$, $\mathbf{V}^{(r)} = \mathbf{v}^{(l)}(\mathbf{v}^{(l)})^H$, $t_1^{(r)} = \frac{\|\text{tr}(\mathbf{D}\mathbf{R}_1\mathbf{V}^{(r)})\|^2}{\text{tr}(\mathbf{R}_1\mathbf{V}^{(r)})}$, and $t_2^{(r)} = \frac{\|\text{tr}(\mathbf{D}\mathbf{R}_2\mathbf{V}^{(r)})\|^2}{\text{tr}(\mathbf{R}_2\mathbf{V}^{(r)})}$
3) **Repeat**:
i) Construct function $\hat{f}_1^{(r)}(\mathbf{V}, t_1, t_2)$ using $\mathbf{V}^{(r)}$, $t_1^{(r)}$, and $t_2^{(r)}$
ii) Solve problem (P3.3) under given $\mathbf{R}_x^{(l)}$ to obtain the optimal solution as $\mathbf{V}^{(r+1)}$, $t_1^{(r+1)}$, and $t_2^{(r+1)}$
iii) Update $r = r + 1$
4) **Until** the convergence criterion is met or the maximum number of inner iterations is reached
5) Reconstruct an approximate rank-one solution $\mathbf{v}^{(l+1)}$ via (39) based on the Gaussian randomization
6) Update $l = l + 1$
c) **Until** the convergence criterion is met or the maximum number of outer iterations is reached

objective value of (P3) [33], [34], thus leading a monotonically non-increasing CRB normally. Otherwise, the outer iteration is terminated. As a result, the convergence of the proposed alternating optimization based algorithm for solving problem (P1) is ensured.

V. TRANSMIT BEAMFORMING OPTIMIZATION FOR CRB MINIMIZATION WITH EXTENDED TARGET

We now optimize the transmit beamforming at the AP to minimize the CRB for estimating the target response matrix in (26) in the extended target case, subject to a maximum transmit power constraint at the AP. Based on Proposition 2, we focus on the scenario with rank($\mathbf{G}_t$) = rank($\mathbf{G}_r$) = N, in order for CRB($\mathbf{H}$) to be bounded or $\mathbf{H}$ to be estimated. As a result, $M_r \geq N$ and $M_t \geq N$. Based on (26), minimizing CRB($\mathbf{H}$) is equivalent to minimizing $\text{tr}((\mathbf{G}_t\mathbf{R}_x\mathbf{G}_t^H)^{-1})$. As a result, the CRB minimization problem for the extended target case is formulated as

$$(\text{P4}): \quad \min_{\mathbf{R}_x} \quad \text{tr}((\mathbf{G}_t\mathbf{R}_x\mathbf{G}_t^H)^{-1})$$

$$\text{s.t.} \quad \text{tr}(\mathbf{R}_x) \leq P_0 \tag{40a}$$

$$\mathbf{R}_x \succeq \mathbf{0}. \tag{40b}$$

We obtain the optimal solution to the convex problem (P4) in closed-form in the following.

Let the SVD of $\mathbf{G}_t$ be denoted by $\mathbf{G}_t = \hat{\mathbf{S}}\hat{\boldsymbol{\Sigma}}\hat{\mathbf{Q}}^H$, where $\hat{\mathbf{S}}\hat{\mathbf{S}}^H = \hat{\mathbf{S}}^H\hat{\mathbf{S}} = \mathbf{I}_N$, $\hat{\mathbf{Q}}\hat{\mathbf{Q}}^H = \hat{\mathbf{Q}}^H\hat{\mathbf{Q}} = \mathbf{I}_{M_t}$, and $\hat{\boldsymbol{\Sigma}} = [\hat{\boldsymbol{\Sigma}}_1, \mathbf{0}] \in \mathbb{R}^{N \times M_t}$ with $\hat{\boldsymbol{\Sigma}}_1 = \text{diag}(\hat{\sigma}_1, \ldots, \hat{\sigma}_N)$ and $\hat{\sigma}_1 \geq \ldots \geq \hat{\sigma}_N > 0$. Then we have

$$\text{tr}((\mathbf{G}_t\mathbf{R}_x\mathbf{G}_t^H)^{-1}) = \text{tr}((\hat{\mathbf{S}}\hat{\boldsymbol{\Sigma}}\hat{\mathbf{Q}}^H\mathbf{R}_x\hat{\mathbf{Q}}\hat{\boldsymbol{\Sigma}}^H\hat{\mathbf{S}}^H)^{-1})$$

$$= \text{tr}((\hat{\boldsymbol{\Sigma}}\hat{\mathbf{R}}_x\hat{\boldsymbol{\Sigma}}^H)^{-1}), \tag{41}$$

where

$$\hat{\mathbf{R}}_x = \hat{\mathbf{Q}}^H\mathbf{R}_x\hat{\mathbf{Q}} \tag{42}$$

with $\hat{\mathbf{R}}_x \in \mathbb{C}^{M_t \times M_t}$ and $\hat{\mathbf{R}}_x \succeq \mathbf{0}$. Based on (42), the power constraint in (40a) is rewritten as

$$\text{tr}(\mathbf{R}_x) = \text{tr}(\hat{\mathbf{Q}}^H\mathbf{R}_x\hat{\mathbf{Q}}) = \text{tr}(\hat{\mathbf{R}}_x) \leq P_0. \tag{43}$$

Furthermore, define

$$\hat{\mathbf{R}}_x = \begin{bmatrix} \hat{\mathbf{R}}_{x,1} & \hat{\mathbf{R}}_{x,2} \\ \hat{\mathbf{R}}_{x,2}^H & \hat{\mathbf{R}}_{x,3} \end{bmatrix}, \tag{44}$$

where $\hat{\mathbf{R}}_{x,1} \in \mathbb{C}^{N \times N}$, $\hat{\mathbf{R}}_{x,2} \in \mathbb{C}^{N \times (M_t - N)}$, and $\hat{\mathbf{R}}_{x,3} \in \mathbb{C}^{(M_t - N) \times (M_t - N)}$. By substituting (44) into (41), we have

$$\text{tr}((\mathbf{G}_t\mathbf{R}_x\mathbf{G}_t^H)^{-1}) = \text{tr}((\hat{\boldsymbol{\Sigma}}_1^2\hat{\mathbf{R}}_{x,1})^{-1}). \tag{45}$$

Based on (42), (43), and (44), (P4) is reformulated as

$$(\text{P4.1}): \quad \min_{\hat{\mathbf{R}}_x \in \mathbb{C}^{N \times N}} \quad \text{tr}((\hat{\boldsymbol{\Sigma}}_1^2\hat{\mathbf{R}}_{x,1})^{-1})$$

$$\text{s.t.} \quad \text{tr}(\hat{\mathbf{R}}_{x,1}) + \text{tr}(\hat{\mathbf{R}}_{x,3}) \leq P_0 \tag{46a}$$

$$\hat{\mathbf{R}}_x \succeq \mathbf{0}$$

$$(44). \tag{46b}$$

We next rely on the following lemma [35], [36].

Lemma 4: Let $\mathbf{J} \in \mathbb{C}^{N \times N}$ be a positive-definite Hermitian matrix with the (i, i)-th entry $J_{i,i}$. Then

$$\text{tr}(\mathbf{J}^{-1}) \geq \sum_{i=1}^N \frac{1}{J_{i,i}}, \tag{47}$$

where the inequality is met with equality if and only if $\mathbf{J}$ is diagonal.

Based on Lemma 4, we have the following proposition.

Proposition 3: The optimality of problem (P4.1) is attained when $\hat{\mathbf{R}}_{x,2}$ and $\hat{\mathbf{R}}_{x,3}$ are all zero matrices, and $\hat{\mathbf{R}}_{x,1}$ is diagonal, i.e., $\hat{\mathbf{R}}_{x,1} = \text{diag}(p_1, \ldots, p_N)$, where $p_i \geq 0, \forall i \in \{1, \ldots, N\}$.

Proof: First, assume that $\hat{\mathbf{R}}_x = \begin{bmatrix} \hat{\mathbf{R}}_{x,1} & \hat{\mathbf{R}}_{x,2} \\ \hat{\mathbf{R}}_{x,2}^H & \hat{\mathbf{R}}_{x,3} \end{bmatrix}$ is optimal for problem (P4.1), where $\hat{\mathbf{R}}_{x,2}$ and $\hat{\mathbf{R}}_{x,3}$ are non-zero. Then, we reconstruct an alternative solution $\hat{\mathbf{R}}_x' = \begin{bmatrix} \hat{\mathbf{R}}_{x,1}' & \hat{\mathbf{R}}_{x,2}' \\ \hat{\mathbf{R}}_{x,2}'^H & \hat{\mathbf{R}}_{x,3}' \end{bmatrix}$, where $\hat{\mathbf{R}}_{x,1}' = \frac{P_0}{\text{tr}(\hat{\mathbf{R}}_{x,1})}\hat{\mathbf{R}}_{x,1}$, $\hat{\mathbf{R}}_{x,2}' = \mathbf{0}$, and $\hat{\mathbf{R}}_{x,3}' = \mathbf{0}$. It is easy to show that the alternative solution $\hat{\mathbf{R}}_x'$ satisfies the constraints in (44), (46a), and (46b), and achieves a lower objective value for (P4.1) than that by $\hat{\mathbf{R}}_x$. Therefore, the presumption is not true, and the optimal solution of $\hat{\mathbf{R}}_{x,2}$ and $\hat{\mathbf{R}}_{x,3}$ should be both zero matrices.

Next, suppose that $\hat{\mathbf{R}}_{x,1}$ is not diagonal. Then, we can construct an alternative solution as $\hat{\mathbf{R}}_{x,1}'' = \text{diag}(p_1, \ldots, p_N)$, where p_i is the i-th diagonal element of $\hat{\mathbf{R}}_{x,1}$, $i \in \{1, \ldots, N\}$. Based on Lemma 4, it follows that the objective value achieved by $\hat{\mathbf{R}}_{x,1}''$ is smaller than that by $\hat{\mathbf{R}}_{x,1}$. Therefore, the presumption is not true. As a result, at the optimal solution of problem (P4.1), $\hat{\mathbf{R}}_{x,1}$ should be diagonal. This thus completes the proof. ∎

Based on Proposition 3, the CRB minimization problem in (P4.1) is reformulated as

$$(\text{P4.2}): \quad \min_{p_1, \ldots, p_N} \quad \sum_{i=1}^N \frac{1}{\hat{\sigma}_i^2 p_i}$$

$$\text{s.t.} \quad \sum_{i=1}^{N} p_i \leq P_0 \tag{48a}$$

$$p_i \geq 0, \forall i \in \{1, \ldots, N\}. \tag{48b}$$

Based on the Karush-Kuhn-Tucker (KKT) conditions, the optimal solution to (P4.2) is presented in the following proposition.

Proposition 4: The optimal solution to problem (P4.2) is

$$p_i^{\star} = \frac{\hat{\sigma}_i^{-1}}{\sum_{i=1}^{N} \hat{\sigma}_i^{-1}} P_0, \quad i \in \{1, \ldots, N\}. \tag{49}$$

Proof: See Appendix D. ∎

By combining (42), (44), and Proposition 4, we directly have the following proposition.

Proposition 5: The optimal solution to problem (P4) is given by

$$\mathbf{R}_x^{\star} = \hat{\mathbf{Q}} \hat{\mathbf{R}}_x^{\star} \hat{\mathbf{Q}}^H, \tag{50}$$

where

$$\hat{\mathbf{R}}_x^{\star} = \begin{bmatrix} \frac{\hat{\boldsymbol{\Sigma}}_1^{-1} P_0}{\sum_{i=1}^{N} \hat{\sigma}_i^{-1}} & \mathbf{0} \\ \mathbf{0} & \mathbf{0} \end{bmatrix}. \tag{51}$$

The resultant CRB is

$$\text{CRB}(\mathbf{H})^{\text{opt}} = \frac{\sigma_{\text{R}}^2 (\sum_{i=1}^{N} \hat{\sigma}_i^{-1})^2}{P_0 T} \text{tr}((\mathbf{G}_r^H \mathbf{G}_r)^{-1}). \tag{52}$$

Based on Proposition 5, it is observed that the optimal solution of $\mathbf{R}_x^{\star}$ follows the eigenmode transmission based on the MIMO channel $\mathbf{G}_t$ between the AP and the IRS, together with a channel amplitude inversion power allocation. In particular, the MIMO channel $\mathbf{G}_t$ is first decomposed into a set of parallel sensing subchannels via SVD, and then a channel amplitude inversion power allocation policy is adopted over these sensing subchannels based on their channel amplitudes. Note that the formula in (50) can be viewed as the EVD of the sample covariance matrix $\mathbf{R}_x^{\star}$. Suppose that $\hat{\mathbf{Q}} = [\hat{\mathbf{q}}_1, \ldots, \hat{\mathbf{q}}_N]$ in (50). Then, based on (2), $\mathbf{R}_x^{\star}$ in (50) corresponds to that the AP transmits N sensing beams, denoted by $\sqrt{p_i^{\star}} \hat{\mathbf{q}}_i, i \in \{1, \ldots, N\}$.

It is interesting to compare the optimal solution $\mathbf{R}_x^{\star}$ in (50) for CRB minimization with IRS versus the optimal isotropic transmission solution $\mathbf{R}_x^{\text{iso}} = P_0 \mathbf{I}_{M_t}/M_t$ without IRS in [20]. With $\mathbf{R}_x^{\text{iso}}$, the resultant CRB for estimating the target response matrix $\mathbf{H}$ is given by

$$\text{CRB}(\mathbf{H})^{\text{iso}} = \frac{\sigma_{\text{R}}^2 M_t \sum_{i=1}^{N} \hat{\sigma}_i^{-2}}{P_0 T} \text{tr}((\mathbf{G}_r^H \mathbf{G}_r)^{-1}) \tag{53a}$$

$$\overset{(a_1)}{\geq} \frac{\sigma_{\text{R}}^2 N \sum_{i=1}^{N} \hat{\sigma}_i^{-2}}{P_0 T} \text{tr}((\mathbf{G}_r^H \mathbf{G}_r)^{-1}) \tag{53b}$$

$$\overset{(a_2)}{\geq} \frac{\sigma_{\text{R}}^2 (\sum_{i=1}^{N} \hat{\sigma}_i^{-1})^2}{P_0 T} \text{tr}((\mathbf{G}_r^H \mathbf{G}_r)^{-1}) = \text{CRB}(\mathbf{H})^{\text{opt}}, \tag{53c}$$

where the inequality (a_1) holds due to the fact that $M_t \geq N$, and the inequality (a_2) holds due to the Jensen's inequality. Notice that in (53), (a_1) and (a_2) are met with equalities if and only if $M = N$ and $\hat{\sigma}_1 = \hat{\sigma}_2 = \cdots = \hat{\sigma}_N$. With $\mathbf{R}_x^{\star}$ in this case, the radiated signals $\boldsymbol{\Phi}\mathbf{G}_t\mathbf{x}(t)$ by the IRS (after reflection) are is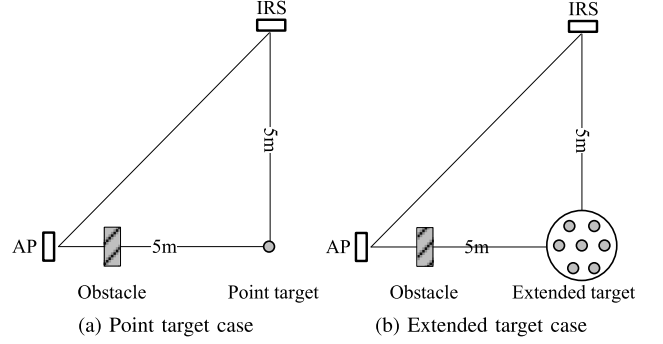otropic, which is thus consistent with the optimality of the isotropic transmission in conventional wireless sensing system without IRS [20].

Fig. 2. Simulation setup.

VI. NUMERICAL RESULTS

This section provides numerical results to evaluate the performance of our proposed joint beamforming design based on CRB minimization. We consider a monostatic MIMO radar scenario with $M_t = M_r$. The distance-dependent path loss is modeled as

$$L(d) = K_0 \left(\frac{d}{d_0} \right)^{-\alpha_0}, \tag{54}$$

where d is the distance of the transmission link and $K_0 = -30$ dB is the path loss at the reference distance $d_0 = 1$ m, and the path-loss exponent α_0 is set as 2.5 for the AP-IRS and IRS-target links. As shown in Fig. 2, the AP and IRS are located at coordinate $(0, 0)$ and $(5\,\text{m}, 5\,\text{m})$, respectively. For the point target case, the target is located at coordinate $(5\,\text{m}, 0)$ (i.e., the target's DoA is $\theta = 0°$ w.r.t. the IRS), with a unit RCS. For the extended target case, we model the extended target as $N_s = 7$ resolvable scatterers uniformly distributed in a circle with radius 0.5 m and center point $(5\,\text{m}, 5\,\text{m})$, with a unit RCS for each scatterer. In this case, the target response matrix is modeled as

$$\mathbf{H} = \sum_{i=1}^{N_s} \alpha_i \mathbf{a}(\theta_i) \mathbf{a}^T(\theta_i), \tag{55}$$

where α_i and θ_i are the reflection coefficient and the DoA of the i-th scatterer, respectively. We consider the Rician fading channel for the AP-IRS and IRS-AP links, i.e.,

$$\mathbf{G}_t = \sqrt{\frac{\beta_{\text{AI}}}{1 + \beta_{\text{AI}}}} \mathbf{G}_t^{\text{LoS}} + \sqrt{\frac{1}{1 + \beta_{\text{AI}}}} \mathbf{G}_t^{\text{NLoS}}, \tag{56}$$

$$\mathbf{G}_r = \sqrt{\frac{\beta_{\text{AI}}}{1 + \beta_{\text{AI}}}} \mathbf{G}_r^{\text{LoS}} + \sqrt{\frac{1}{1 + \beta_{\text{AI}}}} \mathbf{G}_r^{\text{NLoS}}, \tag{57}$$

where $\beta_{\text{AI}} = 0.5$ is the Rician factor, and $\mathbf{G}_t^{\text{LoS}}, \mathbf{G}_r^{\text{LoS}}$ and $\mathbf{G}_t^{\text{NLoS}}, \mathbf{G}_r^{\text{NLoS}}$ are the LoS and NLoS (Rayleigh fading) components, respectively. We set the radar dwell time as $T = 256$. We set the spacing between consecutive reflecting elements at the IRS as half wavelength, i.e., $d_{\text{IRS}} = \lambda_{\text{R}}/2$. We also set the noise power at the AP as $\sigma_{\text{R}}^2 = -120$ dBm. In the simulation, the results are obtained by averaging over 100 realizations, unless otherwise mentioned.
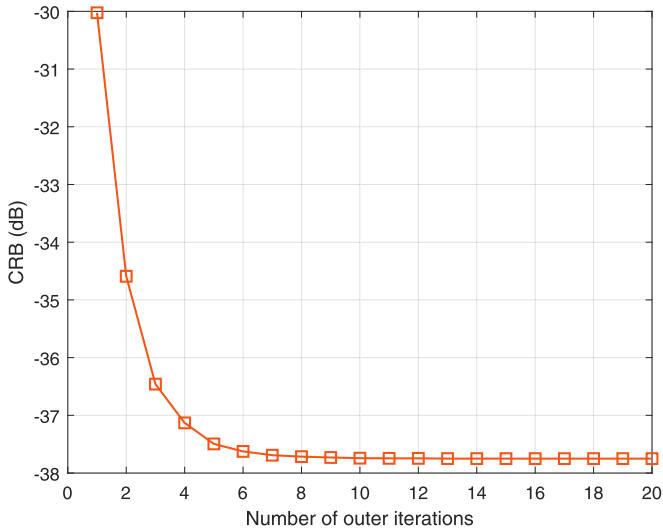
Fig. 3. Convergence behavior of the proposed alternating optimization based algorithm for solving problem (P1), where $P_0 = 30$ dBm, $M_t = M_r = 8$, and $N = 8$.
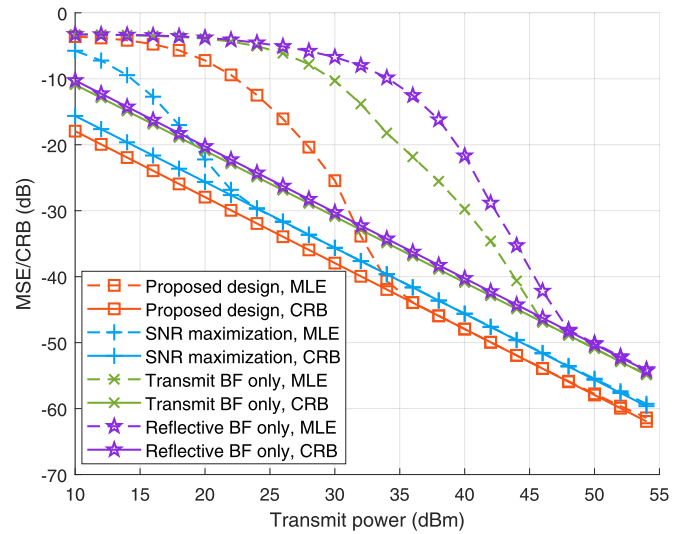

Fig. 4. The MSE/CRB for DoA estimation versus the transmit power P_0 at the AP in point target case, where $M_t = M_r = 8$ and $N = 8$.

A. Point Target Case

First, we consider the point target case. Fig. 3 shows the convergence behavior of our proposed alternating optimization based algorithm for solving problem (P1), where $P_0 = 30$ dBm, $M_t = M_r = 8$, and $N = 8$. It is observed that the proposed alternating optimization based algorithm (Algorithm 1) converges within around 15 outer iterations, thus validating its effectiveness.

Next, we evaluate the estimation performance of our proposed joint beamforming design based on CRB minimization for IRS-enabled sensing as compared to the following benchmark schemes.

1) SNR Maximization: We maximize the SNR of signal radiated from the IRS towards the desired direction, by jointly optimizing the transmit beamforming at the AP and reflective beamforming at the IRS. The average SNR of the radiated signal from the IRS is

$$
\gamma = \frac{1}{T} \sum_{t=1}^{T} \frac{|\mathbf{a}^T \mathbf{\Phi} \mathbf{G}_t \mathbf{x}(t)|^2}{\sigma^2}
$$

$$
= \frac{1}{T} \sum_{t=1}^{T} \frac{|\mathbf{v}^T \mathbf{A}^T \mathbf{G}_t \mathbf{x}(t)|^2}{\sigma^2}
$$

$$
= \frac{\mathrm{tr}((\mathbf{G}_t^T \mathbf{A} \mathbf{v})^* (\mathbf{G}_t^T \mathbf{A} \mathbf{v})^T \mathbf{R}_x)}{\sigma^2}, \tag{58}
$$

where σ^2 is the noise power.

Then, with any given reflective beamformer $\mathbf{v}$, it is well established that maximum-ratio transmission is the optimal transmit beamforming solution, i.e.,

$$
\mathbf{R}_x^{\mathrm{MRT}} = \frac{P_0 \mathbf{G}_t^H \mathbf{A}^* \mathbf{v}^* \mathbf{v}^T \mathbf{A}^T \mathbf{G}_t}{\|\mathbf{G}_t^T \mathbf{A} \mathbf{v}\|^2}. \tag{59}
$$

By substituting $\mathbf{R}_x^{\mathrm{MRT}}$ in (59) into (58), we have the SNR as

$$
\gamma = \frac{P_0 \|\mathbf{G}_t^T \mathbf{A} \mathbf{v}\|^2}{\sigma^2}. \tag{60}
$$

Finally, we optimize the reflective beamforming $\mathbf{v}$ at the IRS to maximize $\|\mathbf{G}_t^T \mathbf{A} \mathbf{v}\|^2$ for equivalently maximizing γ in (60), subject to the unit-modulus constraint in (29d). This is similar to the SNR maximization problem in IRS-enabled multiple-input single-output (MISO) communications that has been studied in [5].

2) Reflective Beamforming Only With Isotropic Transmission (Reflective BF Only): The AP uses the isotropic transmission by transmitting orthonormal signal beams and setting $\mathbf{R}_x = P_0/M_t \mathbf{I}_{M_t}$. Then, the reflective beamforming at the IRS is optimized to minimize $\mathrm{CRB}(\theta)$ in (19) by solving problem (P3).

3) Transmit Beamforming Only With Random Phase Shifts (Transmit BF Only): We consider the random reflecting phase shifts at the IRS, based on which the transmit beamforming at the AP is optimized to minimize $\mathrm{CRB}(\theta)$ in (16) by solving problem (P2).

Furthermore, note that besides the CRB, we also implement the practical MLE method to estimate the target's DoA θ, and accordingly evaluate the MSE as the performance metric for gaining more insights. For brevity, please refer to Appendix E for the details of MLE for the point target case.

Fig. 4 shows the CRB and the MSE with MLE versus the transmit power P_0 at the AP. It is observed that the CRB in decibels (dB) is monotonically decreasing in a linear manner w.r.t. the transmit power P_0 in dB at the AP. This is because that the $\mathrm{CRB}(\theta)$ in (16) is inversely proportional to the transmit power P_0. It is also observed that at the high SNR regime, the derived CRB is identical to the MSE with MLE. This is consistent with the results in [17], [37] and validates the correctness of our CRB derivation. It is also observed that the proposed CRB minimization scheme achieves the lowest CRB in the whole transmit power regime, which shows the effectiveness of our proposed joint beamforming design in CRB minimization. Furthermore, when the transmit power is sufficiently high (e.g., $P_0 > 34$ dBm), the proposed CRB minimization scheme is observed to achieve lower MSE than the three benchmark schemes. When the transmit power is low (e.g., $P_0 < 34$ dBm), the SNR maximization scheme is observed to achieve lower MSE (with
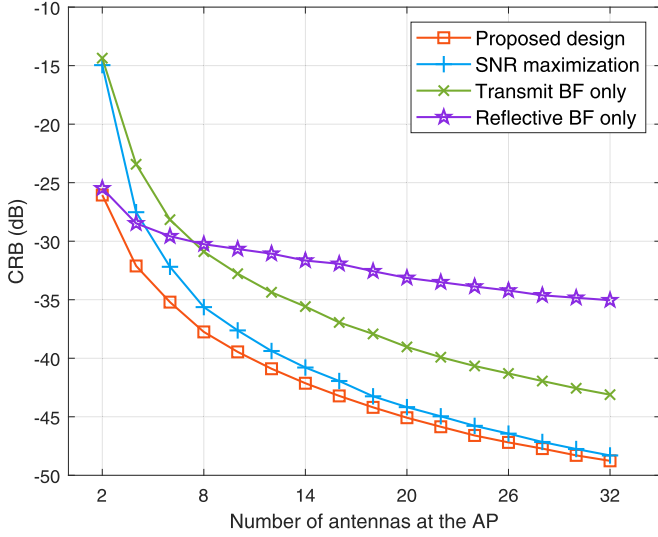
Fig. 5. The CRB for DoA estimating versus the number of antennas $M = M_t = M_r$ at the AP in the point target case, where $P_0 = 30$ dBm and $N = 8$.
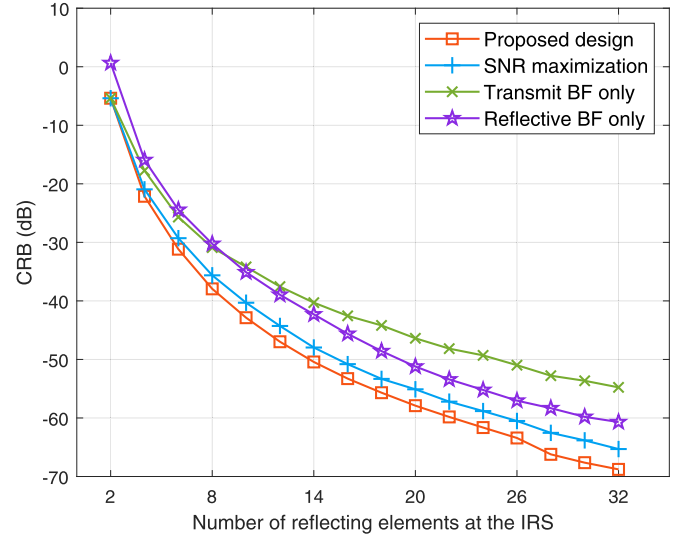

Fig. 6. The CRB for DoA estimation versus the number of reflecting elements N at the IRS in the point target case, where $P_0 = 30$ dBm and $M_t = M_r = 8$.

MLE) than the proposed CRB minimization scheme. This is because that in this case, the CRB is not achievable using MLE, and the estimation performance of MLE is particularly sensitive to the power of echo signals, thus making the SNR maximization scheme desirable.

Fig. 5 shows the CRB for DoA estimation versus the number of antennas $M = M_t = M_r$ at the AP. It is observed that the proposed CRB minimization scheme achieves the lowest CRB in the whole number of antennas regime. It is also observed that with the increasing of the number of antennas M at the AP, the performance gap between the proposed design and reflective beamforming only scheme increases. This shows that the transmit beamforming optimizing is particularly important when the number of antennas at the AP becomes large. Furthermore, as M becomes large, the performance gap between the proposed design and SNR maximization scheme is observed to decrease. This shows that the two designs become consistent in this case.

Fig. 6 shows the CRB for DoA estimation versus the number of reflecting elements N at the IRS. It is observed that the proposed design with CRB minimization achieves the lowest CRB in the whole regime of N, and the performance gap between the proposed design and the transmit beamforming only scheme increases as N becomes larger. This shows the importance of the reflective beamforming optimization, especially when N becomes large. Furthermore, as N becomes large, the performance gap between the proposed design and the SNR maximization scheme is observed to become more significant.

B. Extended Target Case

Next, we consider the extended target case. We evaluate the estimation performance of our proposed beamforming design based on CRB minimization as compared to the isotropic transmission with $\mathbf{R}_x^{\text{iso}} = P_0 \mathbf{I}_{M_t} / M_t$.

Besides the CRB, we also implement the practical MLE method to estimate the target response matrix $\mathbf{H}$, and accordingly evaluate the MSE as the performance metric for gaining more insights. For brevity, please refer to Appendix F for the details of MLE for the extended target case. Based on (21), the target response matrix estimation problem is a linear estimation
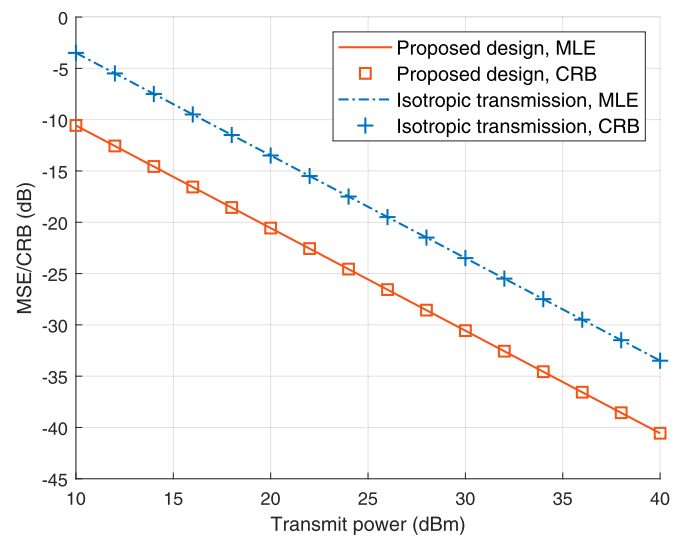

Fig. 7. The MSE/CRB for target response matrix estimation versus the transmit power budget P at the AP in the extended target case, where $M_t = M_r = 8$ and $N = 8$.

model with Gaussian noise. The MLE of target response matrix $\mathbf{H}$ is a minimum variance unbiased (MVU) estimator of $\mathbf{H}$ and the MSE for estimating $\mathbf{H}$ with MLE equals to its CRB [17], [38].

Fig. 7 shows the CRB and the MSE with MLE versus the transmit power P_0 at the AP, where $M_t = M_r = 8$ and $N = 8$. It is observed that similarly as for the point target case, the CRB in dB is monotonically decreasing in a linear manner w.r.t. the transmit power P_0 in dB at the AP. This is because that the CRB($\mathbf{H}$) in (26) is also inversely proportional to the transmit power P_0. It is also observed that the derived CRB is identical to the MSE with MLE, which is consistent with the results in [17], [38] and validates the correctness of the CRB derivation. It is also observed that the proposed CRB minimization scheme achieves the lowest CRB in the whole transmit power regime, which
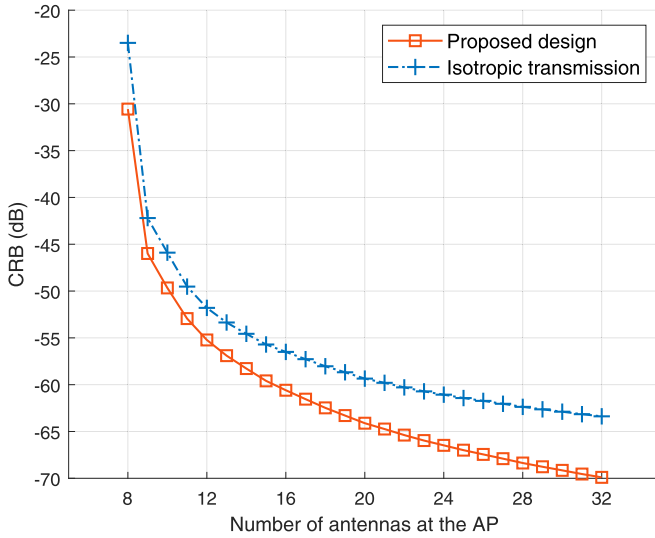
Fig. 8. The CRB for target response matrix estimation versus the number of antennas $M = M_t = M_r$ at the AP in the extended target case, where $P_0 = 30$ dBm and $N = 8$.
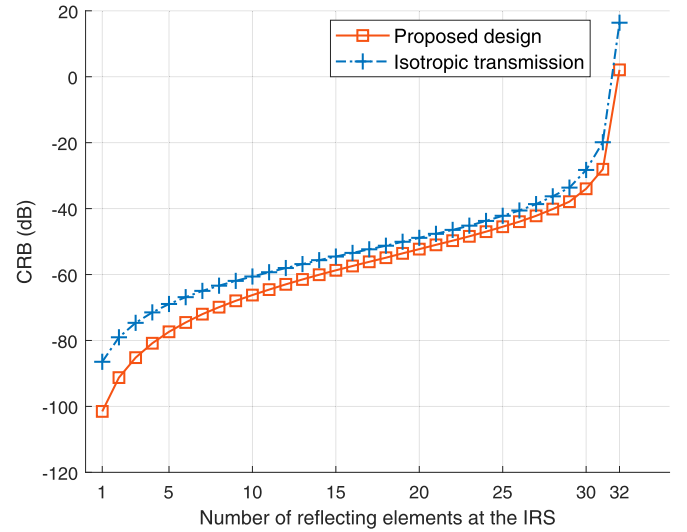

Fig. 9. The CRB for target response matrix estimation versus the number of reflecting elements N at the IRS in the extended target case, where $P_0 = 30$ dBm and $M_t = M_r = 32$.

shows the effectiveness of our proposed transmit beamforming design for CRB minimization.

Fig. 8 shows the CRB for target response matrix estimation versus the number of antennas $M = M_t = M_r$ at the AP. It is observed that the proposed CRB minimization design outperforms the benchmarking isotropic transmission scheme in the whole regime of M, and the performance gap first decreases and then increases as M increases. This can be intuitively explained based on the CRB formulas in (53). In particular, if M_t is much larger than N, then the coefficients M_t in (53a) and N in (53b) dominate $\mathrm{CRB}(\mathbf{H})^{\mathrm{iso}}$ and $\mathrm{CRB}(\mathbf{H})^{\mathrm{opt}}$, respectively. Therefore, the gap between $\mathrm{CRB}(\mathbf{H})^{\mathrm{iso}}$ and $\mathrm{CRB}(\mathbf{H})^{\mathrm{opt}}$ becomes larger as M_t increases in this regime. By contrast, if M_t close to N, then $M_t \sum_{i=1}^{N} \hat{\sigma}_i^{-2}$ in (53a) and $(\sum_{i=1}^{N} \hat{\sigma}_i^{-1})^2$ in (53c) dominate $\mathrm{CRB}(\mathbf{H})^{\mathrm{iso}}$ and $\mathrm{CRB}(\mathbf{H})^{\mathrm{opt}}$, respectively. As the channel amplitude inversions become more indistinct when M_t becomes large, the gap between $M_t \sum_{i=1}^{N} \hat{\sigma}_i^{-2}$ and $(\sum_{i=1}^{N} \hat{\sigma}_i^{-1})^2$ (and thus the gap between $\mathrm{CRB}(\mathbf{H})^{\mathrm{iso}}$ and $\mathrm{CRB}(\mathbf{H})^{\mathrm{opt}}$) decreases as M increases in this regime.

Fig. 9 shows the CRB for target response matrix estimation versus the number of reflecting elements N at the IRS. It is observed that as N becomes larger, the CRB for target response matrix estimation increases due to the increasing number of parameters to be estimated. It is also observed that the proposed design with CRB minimization outperforms the benchmark scheme with isotropic transmission in the whole regime of N, and the performance gap first decreases and then increases as N increases. This can be intuitively explained based on the CRB formulas in (53). In particular, if N is much smaller than M_t, then the coefficients M_t in (53a) and N in (53b) dominate $\mathrm{CRB}(\mathbf{H})^{\mathrm{iso}}$ and $\mathrm{CRB}(\mathbf{H})^{\mathrm{opt}}$, respectively. Therefore, the gap between $\mathrm{CRB}(\mathbf{H})^{\mathrm{iso}}$ and $\mathrm{CRB}(\mathbf{H})^{\mathrm{opt}}$ becomes smaller as N increases in this regime. By contrast, if N becomes larger and close to M_t, then $M_t \sum_{i=1}^{N} \hat{\sigma}_i^{-2}$ in (53a) and $(\sum_{i=1}^{N} \hat{\sigma}_i^{-1})^2$ in (53c) dominate $\mathrm{CRB}(\mathbf{H})^{\mathrm{iso}}$ and $\mathrm{CRB}(\mathbf{H})^{\mathrm{opt}}$, respectively. As the channel amplitude inversions become more distinct when N

becomes large, the gap between $M_t \sum_{i=1}^{N} \hat{\sigma}_i^{-2}$ and $(\sum_{i=1}^{N} \hat{\sigma}_i^{-1})^2$ (and thus the gap between $\mathrm{CRB}(\mathbf{H})^{\mathrm{iso}}$ and $\mathrm{CRB}(\mathbf{H})^{\mathrm{opt}}$) becomes more significant as N increases in this regime.

VII. CONCLUDING REMARKS

This article considered an IRS-enabled NLoS wireless sensing system consisting of an AP with multiple antennas, an ULA-IRS with multiple reflecting elements, and a target at the NLoS region of the AP. We treat two types of target models, namely point and extended target models. The AP aimed to estimate the target's DoA and the target response matrix in the two cases, respectively. We first derived the closed-form CRB expressions for parameters estimation. Then, based on the derived results, we optimized the transmit beamforming at the AP and the reflective beamforming at the IRS to minimize the obtained CRB, subject to a maximum power constraint at the AP. Numerical results showed that the proposed CRB minimization scheme achieved the lowest CRB and MSE with MLE, as compared to other traditional benchmark schemes.

There are several interesting issues unaddressed in this article, which are discussed in the following to motivate future work. In practice, when the number of reflecting elements N becomes large, we may have the rank of AP-IRS or IRS-AP channel is less than the number of reflecting elements, such that the FIM for estimating the whole target response matrix is singular, thus leading to infinite CRB for extended target. How to extend our proposed designs in such a case is generally a challenging task. Towards this end, we can exploit new CRB analysis frameworks for parameter estimation with singular FIM (see, e.g., [39], [40], [41]). In particular, one possible route is to add additional constraints on the parameters to be estimated. Furthermore, the case when the target direction θ is not known or just known to be within a certain region is another interesting direction. On possible solution is to first estimate the complete target response matrix $\mathbf{H}$, and then extract θ from the estimated $\mathbf{H}$. An alternative solution is to employ the idea of worst-case optimization [42] based on the pre-known region of θ. Finally, the

extension of the proposed designs to the more general scenario when the direct link exists is another interesting direction.

APPENDIX A
THE DERIVATION OF THE FIM IN (11)

The covariance matrix $\mathbf{R}_n$ of noise $\tilde{\mathbf{n}}$ is independent of $\boldsymbol{\xi}$. Therefore, we have $\frac{\partial \mathbf{R}_n}{\partial \boldsymbol{\xi}_i} = 0, i = 1, 2, 3$, in (10). Furthermore,

$$\frac{\partial \tilde{\mathbf{u}}}{\partial \theta} = \alpha \mathrm{vec}(\dot{\mathbf{B}}\mathbf{X}), \tag{61}$$

$$\frac{\partial \tilde{\mathbf{u}}}{\partial \tilde{\alpha}} = [1, j] \otimes \mathrm{vec}(\mathbf{B}\mathbf{X}). \tag{62}$$

Accordingly, it follows that

$$\tilde{\mathbf{F}}_{\theta\theta} = \frac{2}{\sigma_R^2} \mathrm{Re}\{(\alpha \mathrm{vec}(\dot{\mathbf{B}}\mathbf{X}))^H \alpha \mathrm{vec}(\dot{\mathbf{B}}\mathbf{X})\}$$

$$= \frac{2|\alpha|^2}{\sigma_R^2} \mathrm{Re}\{\mathrm{tr}(\dot{\mathbf{B}}\mathbf{X})^H(\dot{\mathbf{B}}\mathbf{X})\}$$

$$= \frac{2T|\alpha|^2}{\sigma_R^2} \mathrm{tr}(\dot{\mathbf{B}}\mathbf{R}_x \dot{\mathbf{B}}^H), \tag{63}$$

$$\tilde{\mathbf{F}}_{\theta\tilde{\alpha}} = \frac{2}{\sigma_R^2} \mathrm{Re}\{(\alpha \mathrm{vec}(\dot{\mathbf{B}}\mathbf{X}))^H [1, j] \otimes \mathrm{vec}(\mathbf{B}\mathbf{X})\}$$

$$= \frac{2}{\sigma_R^2} \mathrm{Re}\{\alpha^*[1, j] \otimes (\mathrm{vec}(\dot{\mathbf{B}}\mathbf{X})^H \mathrm{vec}(\mathbf{B}\mathbf{X}))\}$$

$$= \frac{2}{\sigma_R^2} \mathrm{Re}\{\alpha^*[1, j] (\mathrm{tr}(\dot{\mathbf{B}}\mathbf{X})^H \mathbf{B}\mathbf{X})\}$$

$$= \frac{2T}{\sigma_R^2} \mathrm{Re}\{\alpha^* \mathrm{tr}(\mathbf{B}\mathbf{R}_x \dot{\mathbf{B}}^H)[1, j]\}, \tag{64}$$

$$\tilde{\mathbf{F}}_{\tilde{\alpha}\tilde{\alpha}} = \frac{2}{\sigma_R^2} \mathrm{Re}\{([1, j] \otimes \mathrm{vec}(\mathbf{B}\mathbf{X}))^H ([1, j] \otimes \mathrm{vec}(\mathbf{B}\mathbf{X}))\}$$

$$= \frac{2}{\sigma_R^2} \mathrm{Re}\{([1, j]^H [1, j]) \otimes (\mathrm{vec}(\mathbf{B}\mathbf{X})^H \mathrm{vec}(\mathbf{B}\mathbf{X}))\}$$

$$= \frac{2}{\sigma_R^2} \mathrm{Re}\{([1, j]^H [1, j]) \mathrm{tr}((\mathbf{B}\mathbf{X})^H \mathbf{B}\mathbf{X})\}$$

$$= \frac{2T}{\sigma_R^2} \mathrm{tr}(\mathbf{B}\mathbf{R}_x \mathbf{B}^H)\mathbf{I}_2, \tag{65}$$

and the FIM $\tilde{\mathbf{F}}$ in (11) is obtained.

APPENDIX B
PROOF OF PROPOSITION 1

We obtain the determinant of the FIM $\tilde{\mathbf{F}}$ in (11) to present whether $\tilde{\mathbf{F}}$ is invertible or not. Based on (2), (11), (12), (13), and (14), we have

$$\det(\tilde{\mathbf{F}})$$

$$= \frac{8T^3|\alpha|^2}{\sigma^6} \left(\mathrm{tr}(\mathbf{B}\mathbf{R}_x \mathbf{B}^H)\mathrm{tr}(\dot{\mathbf{B}}\mathbf{R}_x \dot{\mathbf{B}}^H) - |\mathrm{tr}(\mathbf{B}\mathbf{R}_x \dot{\mathbf{B}}^H)|^2 \right)$$

$$= \frac{8T^3|\alpha|^2}{\sigma^6} \left((\mathbf{b}^H \mathbf{R}_x^* \mathbf{b})^2 \left(\|\mathbf{c}\|^2 \|\dot{\mathbf{c}}\|^2 - |\dot{\mathbf{c}}^H \mathbf{b}|^2 \right) \right.$$

$$\left. + \|\mathbf{c}\|^4 \left(\dot{\mathbf{b}}^H \mathbf{R}_x^* \mathbf{b}\mathbf{b}^H \mathbf{R}_x^* \mathbf{b} - |\dot{\mathbf{b}}^H \mathbf{R}_x^* \mathbf{b}|^2 \right) \right)$$

$$= \frac{8T^3|\alpha|^2}{\sigma^6} \left(\|(\mathbf{W}\boldsymbol{\Lambda}^{1/2})^T \mathbf{b}\|^4 (\|\dot{\mathbf{c}}\|^2 \|\mathbf{c}\|^2 - |\dot{\mathbf{c}}^H \mathbf{c}|^2) \right.$$

$$+ \|\mathbf{b}\|^4 (\|(\mathbf{W}\boldsymbol{\Lambda}^{1/2})^T \dot{\mathbf{b}}\|^2 \|(\mathbf{W}\boldsymbol{\Lambda}^{1/2})^T \mathbf{b}\|^2$$

$$\left. - |\dot{\mathbf{b}}^H (\mathbf{W}\boldsymbol{\Lambda}^{1/2})^* (\mathbf{W}\boldsymbol{\Lambda}^{1/2})^T \mathbf{b}|^2) \right). \tag{66}$$

When $\mathrm{rank}(\mathbf{G}_t) = \mathrm{rank}(\mathbf{G}_t) = 1$, the truncated SVD of $\mathbf{G}_t$ and $\mathbf{G}_t$ are expressed as $\mathbf{G}_t = \sigma_{1,t}\mathbf{s}_{1,t}\mathbf{q}_{1,t}^T$ and $\mathbf{G}_r = \sigma_{1,r}\mathbf{s}_{1,r}\mathbf{q}_{1,r}^T$, where $\mathbf{s}_{1,t}, \mathbf{s}_{1,r}$ and $\mathbf{q}_{1,t}, \mathbf{q}_{1,r}$ are the left and right dominant singular vectors, and $\sigma_{1,t}, \sigma_{1,r}$ are the dominant singular values of the corresponding matrices. It follows that

$$\mathbf{c} = \sigma_{1,r}\mathbf{q}_{1,r}\mathbf{s}_{1,r}^T \mathbf{A}\mathbf{v}, \tag{67}$$

$$\dot{\mathbf{c}} = j2\pi \frac{d_{\mathrm{IRS}}}{\lambda_R} \cos\theta \sigma_{1,r}\mathbf{q}_{1,r}\mathbf{s}_{1,r}^T \mathbf{A}\mathbf{D}\mathbf{v}, \tag{68}$$

$$(\mathbf{W}\boldsymbol{\Lambda}^{1/2})^T \mathbf{b} = (\mathbf{W}\boldsymbol{\Lambda}^{1/2})^T \sigma_{1,t}\mathbf{q}_{1,t}\mathbf{s}_{1,t}^T \mathbf{A}\mathbf{v}, \tag{69}$$

$$(\mathbf{W}\boldsymbol{\Lambda}^{1/2})^T \dot{\mathbf{b}} = (\mathbf{W}\boldsymbol{\Lambda}^{1/2})^T j2\pi \frac{d_{\mathrm{IRS}}}{\lambda_R} \cos\theta \sigma_{1,t}\mathbf{q}_{1,t}\mathbf{s}_{1,t}^T \mathbf{A}\mathbf{D}\mathbf{v}. \tag{70}$$

It is clear that $\dot{\mathbf{c}}$ and $\mathbf{c}$ are aligned with each other, i.e.,

$$\dot{\mathbf{c}} = \frac{j2\pi d_{\mathrm{IRS}} \cos\theta \mathbf{s}_{1,r}^T \mathbf{A}\mathbf{D}\mathbf{v}}{\lambda_R \mathbf{s}_{1,r}^T \mathbf{A}\mathbf{v}} \mathbf{c}, \tag{71}$$

such that

$$|\dot{\mathbf{c}}^H \mathbf{c}|^2 = \|\dot{\mathbf{c}}\|^2 \|\mathbf{c}\|^2. \tag{72}$$

Similarly, as $(\mathbf{W}\boldsymbol{\Lambda}^{1/2})^T \dot{\mathbf{b}}$ and $(\mathbf{W}\boldsymbol{\Lambda}^{1/2})^T \mathbf{b}$ are aligned with each other, we have

$$|\dot{\mathbf{b}}^H (\mathbf{W}\boldsymbol{\Lambda}^{1/2})^* (\mathbf{W}\boldsymbol{\Lambda}^{1/2})^T \mathbf{b}|^2$$

$$= \|(\mathbf{W}\boldsymbol{\Lambda}^{1/2})^T \dot{\mathbf{b}}\|^2 \|(\mathbf{W}\boldsymbol{\Lambda}^{1/2})^T \mathbf{b}\|^2. \tag{73}$$

Based on (66), (72), and (73), $\det(\tilde{\mathbf{F}}) = 0$, which implies that the FIM $\tilde{\mathbf{F}}$ is not invertible. Accordingly, the CRB in (19) is unbounded.

Next, suppose that $\mathrm{rank}(\mathbf{G}_t) > 1$, in this case $(\mathbf{W}\boldsymbol{\Lambda}^{1/2})^T \dot{\mathbf{b}}$ and $(\mathbf{W}\boldsymbol{\Lambda}^{1/2})^T \mathbf{b}$ are not aligned with each other, we have

$$|\dot{\mathbf{b}}^H (\mathbf{W}\boldsymbol{\Lambda}^{1/2})^* (\mathbf{W}\boldsymbol{\Lambda}^{1/2})^T \mathbf{b}|^2$$

$$< \|(\mathbf{W}\boldsymbol{\Lambda}^{1/2})^T \dot{\mathbf{b}}\|^2 \|(\mathbf{W}\boldsymbol{\Lambda}^{1/2})^T \mathbf{b}\|^2. \tag{74}$$

Similarly, when $\mathrm{rank}(\mathbf{G}_r) > 1$, $\dot{\mathbf{c}}$ and $\mathbf{c}$ are not aligned with each other. According to the Cauchy-Schwarz inequality, we have

$$|\dot{\mathbf{c}}^H \mathbf{b}|^2 < \|\dot{\mathbf{c}}\|^2 \|\mathbf{c}\|^2. \tag{75}$$

Based on (66), (74), and (75), $\det(\tilde{\mathbf{F}}) \neq 0$ when $\mathrm{rank}(\mathbf{G}_t) > 1$ or $\mathrm{rank}(\mathbf{G}_r) > 1$, which implies that the FIM $\tilde{\mathbf{F}}$ is invertible. Accordingly, the CRB in (19) is bounded.

APPENDIX C
THE DERIVATION OF THE FIM IN (23)

As the covariance matrix $\mathbf{R}_n$ of noise $\hat{\mathbf{n}}$ is independent with ζ, we have $\frac{\partial \mathbf{R}_n}{\partial \zeta_i} = 0, i = 1, \ldots, 2N^2$, in (10). Furthermore, we have

$$\frac{\partial \hat{\mathbf{u}}}{\partial \mathbf{h}_R} = \mathbf{X}^T \mathbf{G}_t^T \mathbf{\Phi}^T \otimes \mathbf{G}_r \mathbf{\Phi}^T, \qquad (76)$$

$$\frac{\partial \hat{\mathbf{u}}}{\partial \mathbf{h}_I} = j\mathbf{X}^T \mathbf{G}_t^T \mathbf{\Phi}^T \otimes \mathbf{G}_r \mathbf{\Phi}^T. \qquad (77)$$

Accordingly, it follows that

$$\hat{\mathbf{F}}_{\mathbf{h}_R \mathbf{h}_R} = \frac{2T}{\sigma_R^2} \mathrm{Re}\{(\mathbf{X}^T \mathbf{G}_t^T \mathbf{\Phi}^T \otimes \mathbf{G}_r \mathbf{\Phi}^T)^H$$
$$\cdot (\mathbf{X}^T \mathbf{G}_t^T \mathbf{\Phi}^T \otimes \mathbf{G}_r \mathbf{\Phi}^T)\}$$
$$= \frac{2T}{\sigma_R^2} \mathrm{Re}\{(\mathbf{\Phi}^* \mathbf{G}_t^* \mathbf{R}_x^T \mathbf{G}_t^T \mathbf{\Phi}^T) \otimes (\mathbf{\Phi}^* \mathbf{G}_r^H \mathbf{G}_r \mathbf{\Phi}^T)\}. \qquad (78)$$

Similarly, we have

$$\hat{\mathbf{F}}_{\mathbf{h}_I \mathbf{h}_I} = \frac{2T}{\sigma_R^2} \mathrm{Re}\{(\mathbf{\Phi}^* \mathbf{G}_t^* \mathbf{R}_x^T \mathbf{G}_t^T \mathbf{\Phi}^T) \otimes (\mathbf{\Phi}^* \mathbf{G}_r^H \mathbf{G}_r \mathbf{\Phi}^T)\}, \qquad (79)$$

$$\hat{\mathbf{F}}_{\mathbf{h}_I \mathbf{h}_R} = -\hat{\mathbf{F}}_{\mathbf{h}_R \mathbf{h}_I}$$
$$= \frac{2T}{\sigma_R^2} \mathrm{Im}\{(\mathbf{\Phi}^* \mathbf{G}_t^* \mathbf{R}_x^T \mathbf{G}_t^T \mathbf{\Phi}^T) \otimes (\mathbf{\Phi}^* \mathbf{G}_r^H \mathbf{G}_r \mathbf{\Phi}^T)\}. \qquad (80)$$

APPENDIX D
PROOF OF PROPOSITION 3

The Lagrangian of problem (P4.2) is

$$\mathcal{L} = \sum_{i=1}^{N} \frac{1}{\hat{\sigma}_i^2 p_i} + \mu \left(\sum_{i=1}^{N} p_i - P_0\right) - \sum_{i=1}^{N} \eta_i p_i, \qquad (81)$$

where μ and $\eta_i, i \in \{1, \ldots, N\}$, denote the dual variables. Accordingly, the KKT conditions are given by

$$\frac{\partial \mathcal{L}}{\partial p_i} = -\frac{1}{\hat{\sigma}_i^2 p_i^2} + \mu - \eta_i = 0, \forall i \in \{1, .., N\}, \qquad (82)$$

$$\mu\left(\sum_{i=1}^{N} p_i - P_0\right) = 0, \mu \geq 0, \sum_{i=1}^{N} p_i \leq P_0, \qquad (83)$$

$$\eta_i p_i = 0, \eta_i \geq 0, p_i > 0, \forall i \in \{1, .., N\}. \qquad (84)$$

Then the closed-form solution to problem (P4.2) is

$$p_i^\star = \frac{\hat{\sigma}_i^{-1}}{\sum_{i=1}^{N} \hat{\sigma}_i^{-1}} P_0, \quad i \in \{1, \ldots, N\}. \qquad (85)$$

APPENDIX E
MLE FOR ESTIMATING DOA WITH POINT TARGET

Based on (9), the vectorized received signal at the AP is rewritten as

$$\tilde{\mathbf{y}} = \alpha \mathbf{d}(\theta) + \tilde{\mathbf{n}}, \qquad (86)$$

where $\mathbf{d}(\theta) = \mathrm{vec}(\mathbf{BX})$. The likelihood function of $\tilde{\mathbf{y}}$ given $\boldsymbol{\xi}$ is

$$f_{\tilde{\mathbf{y}}}(\tilde{\mathbf{y}}; \boldsymbol{\xi}) = \frac{1}{(\pi \sigma_R^2)^{MT}} \exp\left(-\frac{1}{\sigma_R^2}\|\tilde{\mathbf{y}} - \alpha \mathbf{d}(\theta)\|^2\right). \qquad (87)$$

In this case, maximizing $f_{\tilde{\mathbf{y}}}(\tilde{\mathbf{y}}; \boldsymbol{\xi})$ is equivalent to minimizing $\|\tilde{\mathbf{y}} - \alpha \mathbf{d}(\theta)\|^2$. Hence, the MLE of θ and α is given by

$$(\theta_{\mathrm{MLE}}, \alpha_{\mathrm{MLE}}) = \arg\min_{\theta, \alpha} \|\tilde{\mathbf{y}} - \alpha \mathbf{d}(\theta)\|^2. \qquad (88)$$

Note that under any given θ, the MLE of α is obtained as

$$\alpha_{\mathrm{MLE}} = (\mathbf{d}^H(\theta) \mathbf{d}(\theta))^{-1} \mathbf{d}^H(\theta) \tilde{\mathbf{y}} = \frac{\mathbf{d}^H(\theta) \tilde{\mathbf{y}}}{\|\mathbf{d}(\theta)\|^2}. \qquad (89)$$

By substituting (89) back into (88), we have

$$\|\tilde{\mathbf{y}} - \alpha_{\mathrm{MLE}} \mathbf{d}(\theta)\|^2 = \|\tilde{\mathbf{y}}\|^2 - \frac{|\mathbf{d}^H(\theta) \tilde{\mathbf{y}}|^2}{\|\mathbf{d}(\theta)\|^2}$$
$$= \|\mathrm{vec}(\mathbf{Y})\|^2 - \frac{|\mathrm{vec}(\mathbf{BX})^H \mathrm{vec}(\mathbf{Y})|^2}{\mathrm{vec}(\mathbf{BX})^H \mathrm{vec}(\mathbf{BX})}$$
$$= \|\mathrm{vec}(\mathbf{Y})\|^2 - \frac{|\mathrm{tr}(\mathbf{B}^H \mathbf{YX}^H)|^2}{\mathrm{tr}((\mathbf{BX})^H \mathbf{BX})}$$
$$= \|\mathrm{vec}(\mathbf{Y})\|^2 - \frac{|\mathbf{c}^H \mathbf{YX}^H \mathbf{b}^*|^2}{T \mathrm{tr}(\mathbf{BR}_x \mathbf{B}^H)}$$
$$= \|\mathrm{vec}(\mathbf{Y})\|^2 - \frac{|\mathbf{c}^H \mathbf{YX}^H \mathbf{b}^*|^2}{T\|\mathbf{c}\|^2 \mathbf{b}^H \mathbf{R}_x^T \mathbf{b}}. \qquad (90)$$

As a result, by substituting (90) into (88), the MLE of θ becomes

$$\theta_{\mathrm{MLE}} = \arg\max_{\theta} \frac{|\mathbf{c}^H \mathbf{YX}^H \mathbf{b}^*|^2}{T\|\mathbf{c}\|^2 \mathbf{b}^H \mathbf{R}_x^T \mathbf{b}}, \qquad (91)$$

which can be obtained via exhaustive search over $\left[-\frac{\pi}{2}, \frac{\pi}{2}\right]$.

APPENDIX F
MLE FOR ESTIMATING TARGET RESPONSE MATRIX WITH EXTENDED TARGET

Based on (21), the vectorized received signal at the AP is rewritten as

$$\hat{\mathbf{y}} = \mathbf{Eh} + \hat{\mathbf{n}}, \qquad (92)$$

where $\mathbf{E} = \mathbf{X}^T \mathbf{G}_t^T \mathbf{\Phi}^T \otimes \mathbf{G}_r \mathbf{\Phi}^T$. The likelihood function of $\tilde{\mathbf{y}}$ given $\mathbf{h}$ is

$$f_{\hat{\mathbf{y}}}(\hat{\mathbf{y}}; \mathbf{h}) = \frac{1}{(\pi \sigma_R^2)^{MT}} \exp\left(-\frac{1}{\sigma_R^2}\|\hat{\mathbf{y}} - \mathbf{Eh}\|^2\right). \qquad (93)$$

In this case, maximizing $f_{\hat{\mathbf{y}}}(\hat{\mathbf{y}}; \mathbf{h})$ is equivalent to minimizing $\|\hat{\mathbf{y}} - \mathbf{Eh}\|^2$. Hence, the MLE of $\mathbf{h}$ is given by

$$\mathbf{h}_{\mathrm{MLE}} = \arg\min_{\mathbf{h}} \|\hat{\mathbf{y}} - \mathbf{Eh}\|^2 = (\mathbf{E}^H \mathbf{E})^{-1} \mathbf{E}^H \tilde{\mathbf{y}}. \qquad (94)$$

REFERENCES

[1] X. Song, J. Xu, F. Liu, T. X. Han, and Y. C. Eldar, "Intelligent reflecting surface enabled sensing: Cramér-Rao lower bound optimization," in *Proc. IEEE Globecom Workshops*, 2022, pp. 413–418.

[2] F. Liu, C. Masouros, A. P. Petropulu, H. Griffiths, and L. Hanzo, "Joint radar and communication design: Applications, state-of-the-art, and the road ahead," *IEEE Trans. Commun.*, vol. 68, no. 6, pp. 3834–3862, Jun. 2020.

[3] F. Liu et al., "Integrated sensing and communications: Towards dual-functional wireless networks for 6G and beyond," *IEEE J. Sel. Areas Commun.*, vol. 40, no. 6, pp. 1728–1767, Jun. 2022.

[4] J. A. Zhang et al., "An overview of signal processing techniques for joint communication and radar sensing," *IEEE J. Sel. Topics Signal Process*, vol. 15, no. 6, pp. 1295–1315, Nov. 2021.

[5] Q. Wu and R. Zhang, "Intelligent reflecting surface enhanced wireless network via joint active and passive beamforming," *IEEE Trans. Wireless Commun.*, vol. 18, no. 11, pp. 5394–5409, Nov. 2019.

[6] Q. Wu, S. Zhang, B. Zheng, C. You, and R. Zhang, "Intelligent reflecting surface-aided wireless communications: A tutorial," *IEEE Trans. Commun.*, vol. 69, no. 5, pp. 3313–3351, May 2021.

[7] S. Gong et al., "Toward smart wireless communications via intelligent reflecting surfaces: A contemporary survey," *IEEE Commun. Surv. Tut.*, vol. 22, no. 4, pp. 2283–2314, Jun. 2020.

[8] E. Björnson, H. Wymeersch, B. Matthiesen, P. Popovski, L. Sanguinetti, and E. de Carvalho, "Reconfigurable intelligent surfaces: A signal processing perspective with wireless applications," *IEEE Signal Process Mag.*, vol. 39, no. 2, pp. 135–158, Mar. 2022.

[9] A. Aubry, A. De Maio, and M. Rosamilia, "Reconfigurable intelligent surfaces for N-LOS radar surveillance," *IEEE Trans. Veh. Technol.*, vol. 70, no. 10, pp. 10735–10749, Oct. 2021.

[10] X. Shao, C. You, W. Ma, X. Chen, and R. Zhang, "Target sensing with intelligent reflecting surface: Architecture and performance," *IEEE J. Sel. Areas Commun.*, vol. 40, no. 7, pp. 2070–2084, Jul. 2022.

[11] W. Lu, Q. Lin, N. Song, Q. Fang, X. Hua, and B. Deng, "Target detection in intelligent reflecting surface aided distributed MIMO radar systems," *IEEE Sens. Lett.*, vol. 5, no. 3, Mar. 2021, Art. no. 7000804.

[12] S. Buzzi, E. Grossi, M. Lops, and L. Venturino, "Radar target detection aided by reconfigurable intelligent surfaces," *IEEE Signal Process. Lett.*, vol. 28, pp. 1315–1319, 2021.

[13] S. Buzzi, E. Grossi, M. Lops, and L. Venturino, "Foundations of MIMO radar detection aided by reconfigurable intelligent surfaces," *IEEE Trans. Signal Process.*, vol. 70, pp. 1749–1763, 2022.

[14] X. Song, D. Zhao, H. Hua, T. X. Han, X. Yang, and J. Xu, "Joint transmit and reflective beamforming for IRS-assisted integrated sensing and communication," in *Proc. IEEE Wireless Commun. Netw. Conf. Workshop*, 2022, pp. 189–194.

[15] Z.-M. Jiang et al., "Intelligent reflecting surface aided dual-function radar and communication system," *IEEE Syst. J.*, vol. 16, no. 1, pp. 475–486, Mar. 2022.

[16] R. Liu, M. Li, Y. Liu, Q. Wu, and Q. Liu, "Joint transmit waveform and passive beamforming design for RIS-aided DFRC systems," *IEEE J. Sel. Topics Signal Process.*, vol. 16, no. 5, pp. 995–1010, Aug. 2022.

[17] S. M. Kay, *Fundamentals of Statistical Signal Processing: Estimation Theory*. Englewood Cliffs, NJ, USA: Prentice-hall, 1993.

[18] I. Bekkerman and J. Tabrikian, "Target detection and localization using MIMO radars and sonars," *IEEE Trans. Signal Process.*, vol. 54, no. 10, pp. 3873–3883, Oct. 2006.

[19] J. Li, L. Xu, P. Stoica, K. W. Forsythe, and D. W. Bliss, "Range compression and waveform optimization for MIMO radar: A Cramér-Rao bound based study," *IEEE Trans. Signal Process.*, vol. 56, no. 1, pp. 218–232, Jan. 2008.

[20] F. Liu, Y.-F. Liu, A. Li, C. Masouros, and Y. C. Eldar, "Cramér-Rao bound optimization for joint radar-communication beamforming," *IEEE Trans. Signal Process.*, vol. 70, pp. 240–253, 2022.

[21] H. Hua, X. Song, Y. Fang, T. X. Han, and J. Xu, "MIMO integrated sensing and communication with extended target: CRB-rate tradeoff," in *Proc. IEEE Glob. Commun. Conf.*, 2022, pp. 4075–4080.

[22] M. Bell, "Information theory and radar waveform design," *IEEE Trans. Inf. Theory*, vol. 39, no. 5, pp. 1578–1597, Sep. 1993.

[23] A. Leshem, O. Naparstek, and A. Nehorai, "Information theoretic adaptive radar waveform design for multiple extended targets," *IEEE J. Sel. Topics Signal Process.*, vol. 1, no. 1, pp. 42–55, Jun. 2007.

[24] B. Tang and J. Li, "Spectrally constrained MIMO radar waveform design based on mutual information," *IEEE Trans. Signal Process.*, vol. 67, no. 3, pp. 821–834, Feb. 2019.

[25] H. Hua, J. Xu, and T. X. Han, "Optimal transmit beamforming for integrated sensing and communication," *IEEE Trans. Veh. Technol.*, early access, Mar. 29, 2023, doi: 10.1109/TVT.2023.3262513.

[26] L. Guo, H. Deng, B. Himed, T. Ma, and Z. Geng, "Waveform optimization for transmit beamforming with MIMO radar antenna arrays," *IEEE Trans. Antennas Propag.*, vol. 63, no. 2, pp. 543–552, Feb. 2015.

[27] J. Li and P. Stoica, "An adaptive filtering approach to spectral estimation and SAR imaging," *IEEE Trans. Signal Process.*, vol. 44, no. 6, pp. 1469–1484, Jun. 1996.

[28] R. Schmidt, "Multiple emitter location and signal parameter estimation," *IEEE Trans. Antennas Propag.*, vol. AP-34, no. 3, pp. 276–280, Mar. 1986.

[29] R. Roy and T. Kailath, "ESPRIT-estimation of signal parameters via rotational invariance techniques," *IEEE Trans. Acoust., Speech, Signal Process.*, vol. 37, no. 7, pp. 984–995, Jul. 1989.

[30] B. Zheng, C. You, W. Mei, and R. Zhang, "A survey on channel estimation and practical passive beamforming design for intelligent reflecting surface aided wireless communications," *IEEE Commun. Surveys Tuts.*, vol. 24, no. 2, pp. 1035–1071, Secondquarter 2022.

[31] F. Zhang, *The Schur Complement and Its Applications*, vol. 4. Berlin, Germany: Springer Sci. Bus. Media, 2006.

[32] M. Grant and S. Boyd, "CVX: Matlab software for disciplined convex programming, version 2.1," Mar. 2014. [Online]. Available: http://cvxr.com/cvx

[33] A. M.-C. So, J. Zhang, and Y. Ye, "On approximating complex quadratic optimization problems via semidefinite programming relaxations," *Math. Program.*, vol. 110, no. 1, pp. 93–110, Jun. 2007.

[34] Z.-Q. Luo, W.-K. Ma, A. M.-C. So, Y. Ye, and S. Zhang, "Semidefinite relaxation of quadratic optimization problems," *IEEE Signal Process. Mag.*, vol. 27, no. 3, pp. 20–34, May 2010.

[35] S. Ohno and G. Giannakis, "Capacity maximizing MMSE-optimal pilots for wireless OFDM over frequency-selective block Rayleigh-fading channels," *IEEE Trans. Inf. Theory*, vol. 50, no. 9, pp. 2138–2145, Sep. 2004.

[36] Y. Yang and R. S. Blum, "MIMO radar waveform design based on mutual information and minimum mean-square error estimation," *IEEE Trans. Aerosp. Electron. Syst.*, vol. 43, no. 1, pp. 330–343, Jan. 2007.

[37] M. A. Richards, *Fundamentals of Radar Signal Processing*. New York, NY, USA: McGraw-Hill Educ., 2014.

[38] Z. Du, F. Liu, and Z. Zhang, "Sensing-assisted beam tracking in V2I networks: Extended target case," in *Proc. IEEE Int. Conf. Acoust., Speech Signal Process.*, Singapore, 2022, pp. 8727–8731.

[39] P. Stoica and B. C. Ng, "On the Cramér-Rao bound under parametric constraints," *IEEE Signal Process Lett.*, vol. 5, no. 7, pp. 177–179, Jul. 1998.

[40] P. Stoica and T. Marzetta, "Parameter estimation problems with singular information matrices," *IEEE Trans. Signal Process.*, vol. 49, no. 1, pp. 87–90, Jan. 2001.

[41] Z. Ben-Haim and Y. C. Eldar, "On the constrained Cramér-Rao bound with a singular Fisher information matrix," *IEEE Signal Process Lett.*, vol. 16, no. 6, pp. 453–456, Jun. 2009.

[42] S. Vorobyov, A. Gershman, and Z.-Q. Luo, "Robust adaptive beamforming using worst-case performance optimization: A solution to the signal mismatch problem," *IEEE Trans. Signal Process.*, vol. 51, no. 2, pp. 313–324, Feb. 2003.

Xianxin Song (Graduate Student Member, IEEE) received the B.E. degree from the University of Electronic Science and Technology of China, Chengdu, China, in 2017, and the M.E. degree from the Beijing University of Posts and Telecommunications, Beijing, China, in 2020. He is currently working toward the Ph.D. degree with the School of Science and Engineering and the Future Network of Intelligence Institute, The Chinese University of Hong Kong, Shenzhen, China. His research interests include integrated sensing and communication, intelligent reflecting surface, and edge intelligence.

Jie Xu (Senior Member, IEEE) received the B.E. and Ph.D. degrees from the University of Science and Technology of China in 2007 and 2012, respectively. From 2012 to 2014, he was a Research Fellow with the Department of Electrical and Computer Engineering, National University of Singapore, Singapore. From 2015 to 2016, he was a Post-Doctoral Research Fellow with engineering systems and design pillar, Singapore University of Technology and Design, Singapore. From 2016 to 2019, he was a Professor with the School of Information Engineering, Guangdong University of Technology, Guangzhou, China. He is currently an Associate Professor with the School of Science and Engineering, The Chinese University of Hong Kong, Shenzhen, China. His research interests include wireless communications, wireless information and power transfer, UAV communications, edge computing and intelligence, and integrated sensing and communication (ISAC). He was the recipient of the 2017 IEEE Signal Processing Society Young Author Best Paper Award, the IEEE/CIC ICCC 2019 Best Paper Award, the 2019 IEEE Communications Society Asia-Pacific Outstanding Young Researcher Award, and the 2019 Wireless Communications Technical Committee Outstanding Young Researcher Award. He is the Symposium Co-Chair of the IEEE GLOBECOM 2019 Wireless Communications Symposium, the workshop Co-Chair of several IEEE ICC and GLOBECOM workshops, the Tutorial Co-Chair of the IEEE/CIC ICCC 2019, the Vice Chair of the IEEE Wireless Communications Technical Committee, and the Vice Co-chair of the IEEE Emerging Technology Initiative on ISAC. He is/was serving as the Editor of the IEEE TRANSACTIONS ON WIRELESS COMMUNICATIONS, IEEE TRANSACTIONS ON COMMUNICATIONS, IEEE WIRELESS COMMUNICATIONS LETTERS, and the Journal of Communications and Information Networks. He was an Associate Editor for IEEE ACCESS, and the Guest Editor of the IEEE WIRELESS COMMUNICATIONS, IEEE JOURNAL ON SELECTED AREAS IN COMMUNICATIONS, and Science China Information Sciences.

Fan Liu (Member, IEEE) received the B.Eng. and the Ph.D. degrees from Beijing Institute of Technology (BIT), Beijing, China, in 2013 and 2018, respectively is currently an Assistant Professor of the Department of Electronic and Electrical Engineering, Southern University of Science and Technology (SUSTech). He has previously held academic positions with the University College London, Lomdon, U.K., first as a Visiting Researcher from 2016 to 2018, and then as a Marie Curie Research Fellow from 2018 to 2020. His research interests incllude the general area of signal processing and wireless communications, and in particular in the area of Integrated Sensing and Communications (ISAC). He has 10 publications selected as IEEE ComSoc Besting Readings in ISAC. He is the Founding Academic Chair of the IEEE ComSoc ISAC Emerging Technology Initiative (ISAC-ETI), an Associate Editor for the IEEECOMMUNICATIONS LETTERS and the IEEE OPEN JOURNAL OF SIGNAL PROCESSING, and the Guest Editor of the IEEE JOURNAL ON SELECTED AREAS IN COMMUNICATIONS, IEEE WIRELESS COMMUNICATIONS, and China Communications. He was also an organizer and the Co-Chair of numerous workshops, special sessions and tutorials in flagship IEEE/ACM conferences, including ICC, GLOBECOM, ICASSP, and MobiCom. He is the TPC Co-Chair of the 2nd and 3rd IEEE Joint Communication and Sensing Symposium (JC&S), the Track Chair of the ISAC Track of the IEEE GLOBECOM 2023 Selected Areas in Communications Symposium, and will serve as the Track Co-Chair for the IEEE WCNC 2024. He is a Member of the IMT-2030 (6G) ISAC Task Group. He was the recipient of the 2023 IEEE ComSoc Stephan O. Rice Prize, 2023 IEEE ICC Best Paper Award, 2021 IEEE Signal Processing Society Young Author Best Paper Award, the 2019 Best Ph.D. Thesis Award of Chinese Institute of Electronics, and the 2018 EU Marie Curie Individual Fellowship. Dr. Fan Liu was listed in the World's Top 2% Scientists by Stanford University for citation impact in 2021 and 2022.

Tony Xiao Han (Senior Member, IEEE) received the B.E. degree in electrical engineering from Sichuan University, Chengdu, China, and the Ph.D. degree in communications engineering from Zhejiang University, Hangzhou, China. He is currently a Research Expert and Project Manager with Huawei Technologies Company, Ltd., Shenzhen, China. He was a Postdoctoral Research Fellow with the National University of Singapore, Singapore. His research interests include wireless communications, signal processing, integrated sensing and communication (ISAC), and standardization of wireless communication. Dr. Han was the Chair of IEEE 802.11 WLAN Sensing Topic Interest Group and Chair of 802.11 WLAN Sensing Study Group. He is the Chair of IEEE 802.11bf WLAN Sensing Task Group. He is also the Founding Industry Chair of IEEE ComSoc ISAC Emerging Technology Initiative (ISAC-ETI), Vice Chair of IEEE WTC Special Interest Group on ISAC, Guest Editor of the IEEE JOURNAL ON SELECTED AREAS IN COMMUNICATIONS Special Issue on Integrated Sensing and Communications (ISAC). He was the Co-Chair of many workshops, such as IEEE GLOBECOM 2020 workshop on ISAC.

Yonina C. Eldar (Fellow, IEEE) received the B.Sc. degree in physics and the second B.Sc. degree in electrical engineering from Tel-Aviv University, Tel-Aviv, Israel, in 1995 and 1996, respectively, and the Ph.D. degree in electrical engineering and computer science from the Massachusetts Institute of Technology (MIT), Cambridge, U.K., in 2002. She is currently a Professor with the Department of Mathematics and Computer Science, Weizmann Institute of Science, Rehovot, Israel. She was previously a Professor with the Department of Electrical Engineering, Technion. She is also a Visiting Professor with MIT, Visiting Scientist with the Broad Institute, an Adjunct Professor with Duke University, Durham, NC, USA, and was a Visiting Professor with Stanford University, Stanford, CA, USA. She is the author of the book *Sampling Theory: Beyond Bandlimited Systems* and co-author of five other books published by Cambridge University Press. Her research interests include the broad areas of statistical signal processing, sampling theory and compressed sensing, learning and optimization methods, and their applications to biology, and medical imaging and optics. Dr. Eldar was the recipient of many awards for excellence in research and teaching, including the IEEE Signal Processing Society Technical Achievement Award (2013), IEEE/AESS Fred Nathanson Memorial Radar Award (2014), IEEE Kiyo Tomiyasu Award (2016), the Michael Bruno Memorial Award from the Rothschild Foundation, Weizmann Prize for Exact Sciences, Wolf Foundation Krill Prize for Excellence in Scientific Research, Henry Taub Prize for Excellence in Research (twice), Hershel Rich Innovation Award (three times), Award for Women with Distinguished Contributions, Andre and Bella Meyer Lectureship, Career Development Chair at the Technion, Muriel & David Jacknow Award for Excellence in Teaching, and Technion's Award for Excellence in Teaching (two times). She was also the recipient of the best paper awards and best demo awards together with her research students and colleagues including the SIAM outstanding Paper Prize, UFFC Outstanding Paper Award, Signal Processing Society Best Paper Award, and IET Circuits, Devices and Systems Premium Award. She was selected as one of the 50 most influential women in Israel and in Asia, and is a highly cited Researcher. She is the Editor-in-Chief of *Foundations and Trends in Signal Processing*, a Member of the IEEE Sensor Array and Multichannel Technical Committee and serves on several other IEEE committees. In the past, she was a Signal Processing Society Distinguished Lecturer, Member of the IEEE Signal Processing Theory and Methods and Bio Imaging Signal Processing technical committees, and an Associate Editor for the IEEE TRANSACTIONS ON SIGNAL PROCESSING, *EURASIP Journal of Signal Processing*, *SIAM Journal on Matrix Analysis and Applications*, and *SIAM Journal on Imaging Sciences*. She was the co-chair and technical co-chair of several international conferences and workshops. She is a Member of the Israel Academy of Sciences and Humanities (elected 2017), and an EURASIP Fellow. She is a Horev Fellow of the Leaders in Science and Technology program with the Technion and an Alon Fellow. She is a Member of the Young Israel Academy of Science and Humanities, and the Israel Committee for Higher Education.